Review Article

Nano Research
2022, 15(12): 10328–10342

ISSN 1998-0124 CN 11-5974/O4
https://doi.org/10.1007/s12274-022-4666-y

Insights on catalytic mechanism of CeO_2 as multiple nanozymes

Yuanyuan Ma[§], Zhimin Tian[§], Wenfang Zhai, and Yongquan Qu (✉)

Key Laboratory of Special Functional and Smart Polymer Materials of Ministry of Industry and Information Technology, School of Chemistry and Chemical Engineering, Northwestern Polytechnical University, Xi'an 710072, China
[§] *Yuanyuan Ma and Zhimin Tian contributed equally to this work.*

Received: 28 April 2022 / **Revised:** 14 June 2022 / **Accepted:** 14 June 2022

ABSTRACT

CeO_2 with the reversible Ce^{3+}/Ce^{4+} redox pair exhibits multiple enzyme-like catalytic performance, which has been recognized as a promising nanozyme with potentials for disease diagnosis and treatments. Tailorable surface physicochemical properties of various CeO_2 catalysts with controllable sizes, morphologies, and surface states enable a rich surface chemistry for their interactions with various molecules and species, thus delivering a wide variety of catalytic behaviors under different conditions. Despite the significant progress made in developing CeO_2-based nanozymes and their explorations for practical applications, their catalytic activity and specificity are still uncompetitive to their counterparts of natural enzymes under physiological environments. With the attempt to provide the insights on the rational design of highly performed CeO_2 nanozymes, this review focuses on the recent explorations on the catalytic mechanisms of CeO_2 with multiple enzyme-like performance. Given the detailed discussion and proposed perspectives, we hope this review can raise more interest and stimulate more efforts on this multi-disciplinary field.

KEYWORDS

heterogeneous catalysis, ceria, nanozyme, oxygen vacancy

1 Introduction

Nanozymes, new emerging inorganic nanocatalysts as the alternatives of natural enzymes, mimick the catalytic behavior of natural enzymes and exhibit diverse applications in the field of food science, environmental remediation, clinical diagnosis, and disease therapy [1–6]. This concept is originated from a pioneer investigation of magnetic Fe_3O_4 nanoparticles with the peroxidase-like catalytic performance and their potentials for novel immunoassay with three functions of capture, separation, and detection [7]. In comparison with natural counterparts, nanozymes delivered the unique benefits of the high diversity of structures, cost-effective synthesis, high chemical stability, easy storage, etc. Afterwards, many nanomaterials with various tailorable morphologies, including metals, metal oxides, carbon, metal sulfides, metal organic frameworks, etc., have been developed as nanozymes with many interesting enzyme-like catalytic performance as well as their wide applications [8–25]. Recent reviews have well summarized and documented the great progress of diversiform nanozymes, especially on their design, synthesis, and applications for disease diagnosis and treatments.

Despite the rapid development of nanozymes, their relatively low catalytic activity and poor specificity, especially under the physiological environments, have severely limited their potential applications [1–3, 8, 25]. The concept of nanozymes is an interdisciplinary field, which bridges the disciplines of enzymology and heterogeneous catalysis. To date, the catalytic performance of nanozymes is generally analyzed by the Michaelis–Menten equation, in which two parameters of k_{cat} and K_m are used to describe the catalytic reaction rate and adsorption affinity of substrates on the surfaces of nanozymes, respectively [7, 26–30]. This method is practically adopted to understand the catalytic kinetics of natural enzymes, which cannot accurately reflect the catalytic mechanism of nanozymes. Considering that the nanozymes are solid catalysts with the tailorable surface physicochemical properties, a strong relationship between activity and surface physicochemical properties of solids makes nanozymes being more liking recognized as a new type of heterogeneous catalysts. Similar to heterogeneous catalysis, the nanozymes also go through the adsorption and activations of reactants on the catalyst surfaces, the formation of the intermediates, and the generation and release of products, accompanied with the recovery of surface active center [31–53]. Thus, the surface physicochemical properties and electronic configurations of the catalytic centers significantly affect their catalytic activity and selectivity. However, majority of current investigations of nanozymes focus on their synthesis and applications as sensors, clinic diagnosis, and nanodrugs. The catalytic pathways of nanozymes under the complicated physiological environment of both normal tissues and lesional tissues are far behind the developments of novel materials themselves. The recognitions on the relationships between surface properties and catalytic behaviors of nanozymes at the atomic and electronic levels would significantly benefit their rational design, synthesis, and exploration for diagnosis and therapy of a specific disease.

Among various nanozymes, CeO_2 nanocatalysts with low biotoxicity and high biocompatibility have been identified as

Address correspondence to yongquan@nwpu.edu.cn

promising nanozymes with multiple biomimic activity, including peroxidase, oxidase, catalase, superoxide dismutase (SOD), photolyase, phosphatase, haloperoxidase, etc. [1–5, 32–45, 54–65]. Generally, their diverse enzyme-like activity is ascribed from the highly reversible Ce^{3+}/Ce^{4+} redox pair as well as their surface environments. Afterwards, CeO_2 nanozymes and their composites have been demonstrated to deliver high potentials for early diagnosis and treatments of Parkinson disease, inflammations, as well as various tumor therapies [1–5, 12, 54–56, 66–69]. However, the recognitions on the therapeutic pathways for those applications are very obscure, which is partially accounted to poor understandings on catalytic mechanisms of CeO_2 catalysts and their composites under the complicated operation conditions. Recently, many efforts have been carried out to provide the insights on the catalytic mechanism at atomic/electronic levels, which significantly promotes the rational design and synthesis of CeO_2-based nanozymes towards high activity and specificity.

Raising demands for active, selective, and robust nanozymes for practical applications requires those nanoscaled artificial enzymes with high catalytic activity and specificity comparable to or even better than their counterparts of natural enzymes under the practical operations. However, this gap between nanozymes and natural enzymes is still unsurpassable. Hence, the rational design of nanozymes based on the simulation of the structural characteristics of natural enzymes is an attractive strategy. The tremendous challenges not only require the developments of synthesis of novel nanozymes with new functions, but also stimulate the deep understandings on the catalytic mechanism of nanozymes at atomic/electronic levels. With the attempt to provide the primary cognitions for the rational design of CeO_2-based nanozymes, this review summarizes the recent progress of CeO_2-based nanozymes and focuses on the latest explorations on the catalytic mechanisms of CeO_2 with multiple enzyme-like performance. Accordingly, the crystal structures, surface properties, and relative characterizations of CeO_2 nanostructures are initially introduced. The following section devotes to the enzyme-like activity of CeO_2 with an attempt to illustrate the surface property–activity relationship. In this part, the recent advances on the catalytic mechanism of CeO_2 nanozymes are discussed. Finally, a brief summary and perspectives are presented. We anticipate this review provides fundamental understandings on the catalytic mechanism of CeO_2-based nanozymes, raises wide interest of community, and inspires great efforts on design and synthesis of highly performed CeO_2 catalysts with comparable catalytic performance of natural counterparts.

2 Structures and surface properties of CeO_2

Typically, ideal CeO_2 crystal is featured by a cubic fluorite structure with a face-centered cubic unit cell, in which Ce^{4+} ion is located at the center of a cube composed of eight O^{2-} (Fig. 1(a)) [70]. Thus, each Ce^{4+} is coordinated with eight O^{2-} and each O^{2-} is coordinated with four Ce^{4+} in the lattice. When the size of CeO_2 is reduced to nanoscale, the removal of an oxygen from the crystal lattice becomes much easy due to the dynamically reversible Ce^{3+}/Ce^{4+} redox pair, inducing the generation of one oxygen vacancy accompanied with the alternation of two Ce^{4+} ions into two Ce^{3+} species and thereby giving nonstoichiometric CeO_{2-x} (Fig. 1(b)) [70–72]. Such a structural evolution induces a rich surface chemistry of nanoscale ceria, leading to the co-existence of the interfacial Lewis acidic and basic species as well as Bronsted acidic sites. Besides, the defective CeO_{2-x} catalysts show the features of high oxygen mobility, high surface reducibility, large oxygen storage capacity, etc. Thus, many attractive catalytic behaviors of CeO_{2-x} are discovered, where it is recognized as the

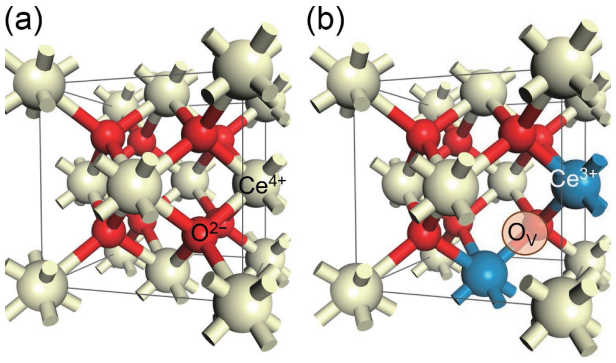

Figure 1 Schematic illustration of CeO_2 structure. (a) Ideal CeO_2. (b) Defective CeO_2 with one oxygen vacancy.

catalytic active components, functional supports, or additives in heterogeneous catalysis [70–83].

The electronic and geometrical configurations of those interfacial species significantly affect the catalytic performance of CeO_2-based catalysts. Considering those species generated from the structural defects of oxygen vacancy, the controllability of the ratios of Ce^{3+}/Ce^{4+} as well as the concentrations of oxygen vacancies becomes critical, in which the surface Ce^{3+} fraction has been widely adopted as the descriptor for their catalytic performance [76–79]. Generally, the abundance of the structural defects of oxygen vacancy shows an evidently size-dependent correlation, in which CeO_{2-x} with smaller size always introduces more oxygen vacancies [84]. Also, how to enable effective and rapid cycling of Ce^{3+}/Ce^{4+} redox pair plays pivotal roles in their catalytic behaviors. Besides, the formation energy of oxygen vacancy displayed as a strong crystal plane dependence in an order of (110) < (100) < (111) [85–88]. Therefore, many synthetic strategies have been developed to prepare the size- and morphological controllable ceria nanostructures as catalysts, including nanorods, porous nanorods, cubes, octahedra, nanosheets, nanotubes, mesoporous particles, etc. Among various synthetic methodology, hydrothermal approach is the facile method to prepare CeO_2 nanostructures with various shapes (rods, cubes, and octahedrons) by tailoring synthetic conditions [41, 89–92]. CeO_2 nanorods are generally enclosed by (110) and (100) facets. While, nanocubes and octahedrons are enclosed by (100) and (111) facets, respectively [42]. They have been widely used as the model catalysts for the surface-depended catalytic behaviors of CeO_2 nanozymes. Various real-time operations and post-treatments on as-synthesized CeO_2 nanostructures, including calcinations, pressure regulations, wet-chemical etching, and irradiations, successfully modulate the surface physicochemical properties of ceria catalysts [42, 60, 61, 70, 93, 94]. More information can be found in previous reviews.

The identification of surface properties of catalysts is the prerequisite for deep understandings on the catalytic mechanism. Generally, the surface properties of CeO_2 can be characterized by several well-established techniques. X-ray photoelectron spectroscopy (XPS) is widely adopted to probe their surface Ce^{3+}-to-Ce^{4+} ratios [2, 41–44, 51, 74, 77]. The derived surface Ce^{3+} fraction is used to index the concentration of oxygen vacancy as well as characterize the chemical/electronic states of various surface species. Raman spectroscopy can characterize the density of oxygen vacancy in CeO_2. Combination of XPS and Raman practically delivers the information of the structural defect of CeO_2 nanostructures [2, 44, 51, 74, 77]. Nuclear magnetic resonance (NMR) spectroscopy is a sensitive technique to qualitatively and quantitatively provide information (e.g., type, concentration, and distribution) of the interfacial acidic and basic sites [36, 95]. Fourier transform infrared (FTIR) spectroscopy gives the

information of the surface adsorbed species of CeO_2 or modified nanozymes [31, 59]. Temperature-programmed reduction/oxidation (TPR/TPO) can give the surface redox situations of CeO_2-based nanozymes with the assistance of probe molecules [71, 72, 77]. X-ray absorption spectroscopy (XAS) techniques, specifically X-ray absorption near-edge structure and extended X-ray absorption fine structure, are generally adopted to characterize the local electronic/geometric structures of defects of CeO_2-based catalysts at the atomic scale [74, 77].

3 Catalytic behaviors of CeO_2 as nanozymes

The capability of CeO_2 for the reversible switch between redox pair of Ce^{3+}/Ce^{4+} has been recognized as the critical parameters to enable CeO_2 with various enzyme-like catalytic performance, as shown in Fig. 2 [1–5, 55]. Their catalytic performance significantly depends on the morphologies, surface abundance of structural defects as well as the catalytic conditions, such as pH, temperatures, and levels of reactive oxygen species (ROS) in the environments [41–43, 55, 60].

3.1 Peroxidase-like activity

Peroxidases as the natural enzymes catalytically generate ROS from H_2O_2 and efficiently enable the oxidation of a number of substrates afterwards. Nanoceria was seldomly reported as peroxidase mimetics in the early stage of nanozymes. It has been reported that nanoceria with a low level of structural defects of oxygen vacancies delivers poor activity due to its weak affinity for H_2O_2 as well as poor activation to generate the active oxygen species [55]. Recently, porous nanorods of ceria (PN-CeO_2) were demonstrated as a highly active and robust artificial peroxidase mimetics, which was attributed to its large surface area and a high level of oxygen vacancy as structural defect [41]. Porous nanorods were prepared via a two-step hydrothermal approach and displayed a rod-like morphological feature with a diameter of

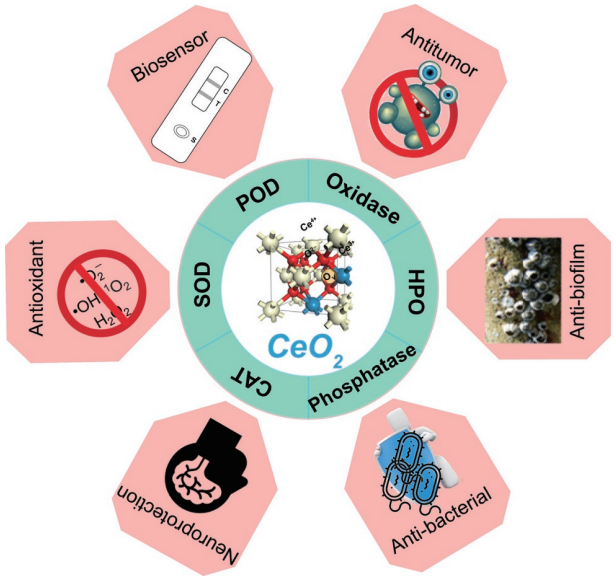

Figure 2 Illustration of various enzyme-like activity of defective ceria and their potential applications.

~ 8 nm, a length of ~ 60 nm, and a pore size of 2–4 nm (Fig. 3(a)). The surface Ce^{3+} fraction of PN-CeO_2 was 33.8%, suggesting the abundant structural defects of nanozymes. With 3,3',5,5'-tetramethylbenzidine (TMB) as reactant and H_2O_2 as oxidant, PN-CeO_2 delivered a surprisingly high catalytic peroxidase activity in comparison with nature enzyme horseradish peroxidase (HRP) under the equal conditions (Fig. 3(b)). Particularly, the barely changed activity of PN-CeO_2 recorded at temperatures from 4 to 60 °C and negligible variety in activity of PN-CeO_2 calcinated at different temperatures from 4 to 200 °C ensure the accuracy and reliability as well as convenience for practical measurements in comparison with natural HRP.

To further explore the origination of PN-CeO_2 as highly

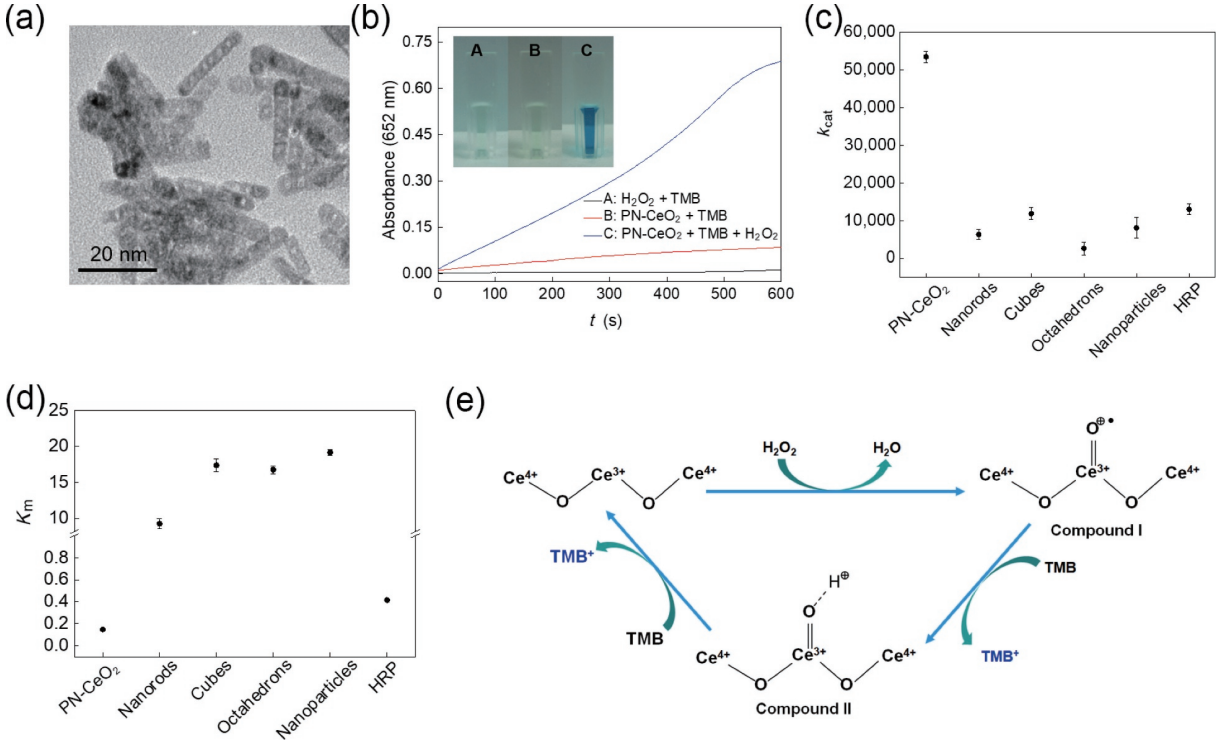

Figure 3 Structures, catalytic activity, and mechanism of PN-CeO_2 as peroxidase mimics. (a) Transmission electron microscopy (TEM) image of PN-CeO_2. (b) Activity of PN-CeO_2. Inset is color change of TMB and H_2O_2 in NaAc buffer (0.2 M, pH = 4.0) under different treatments. (c) The k_{cat} values of various CeO_2 nanozymes and HRP. (d) The K_m of various CeO_2 nanozymes and HRP. (e) Proposed mechanism of CeO_2 nanozymes as peroxidase mimics. Reproduced with permission from Ref. [41], © Elsevier Ltd. 2015.

performed peroxidase mimics, the CeO_2 particles, cubes, octahedrons, and nanorods were also synthesized with the surface Ce^{3+} fractions of 15.9%, 16.7%, 19.0%, and 14.4%, respectively. Kinetically, the Michaelis–Menten curves suggested the apparent K_m value of PN-CeO_2 was only one-third of that of HRP and much lower than other CeO_2, suggesting the higher affinity of TMB on PN-CeO_2 over that on HRP as well as other shaped CeO_2 nanozymes (Fig. 3(c)). Comparatively, k_{cat} of PN-CeO_2 with TMB was 4.1 and 8.4 times larger than those of HRP and nonporous CeO_2 nanorods, indicating the best peroxidase-like performance of PN-CeO_2 nanozymes (Fig. 3(d)). The kinetic studies indicated the high level of structural defects of CeO_2 catalysts enables the high affinity of TMB substrates with the interface active sites. Thus, the surface defective sites could be recognized as the catalytically active centers for the activation and consequential TMB oxidation. The interfacial Ce^{3+} sites are proposed as the catalytic centers for adsorption and activation of H_2O_2 as well as the generation of active oxygen species for the TMB oxidation (Fig. 3(e)). Combining the high affinity of TMB on the highly defective CeO_2 surface, the activity of the peroxidase-like various ceria nanozymes showed a strong defect-depended relationship. The catalytic activity of PN-CeO_2 as artificial peroxidase is also significantly improved by the rapid cycle of the reversible Ce^{3+}/Ce^{4+} redox pair, which could further promote the charge transfer between CeO_2 nanozymes and TMB substrates as well as H_2O_2. Large surface area of CeO_2 nanozymes also provides more active sites for catalytic reaction.

The above investigations indicated a correlation between the structural defects of ceria nanozymes and their catalytic activity as peroxidase mimics [31, 55, 96–100]. The high catalytic activity was found on the CeO_2 nanozymes featured with the high level of the surface Ce^{3+} fraction and large surface area. A recent density functional theory (DFT) calculation suggested that the catalytic activity of the CeO_2 nanozymes as artificial peroxidase was analogy to those of noble metals and iron oxides, which is as follow: (1) adsorption of a molecule of H_2O_2 at the interfacial Ce site; (2) adsorptive dissociation of H_2O_2* into two HO* adsorbates; and (3) and (4) subsequent reduction of two HO* by the two TMB-H^+ molecules (Fig. 4(a)). Further calculations suggest that the dissociative chemisorption of H_2O_2 on CeO_2 is the rate-determined step (Figs. 4(b) and 4(c)) [97]. The kinetic energy barrier of this step is 1.14 eV on the defective CeO_2 surface, where the oxygen vacancy located on the third layer gives the best catalytic performance. In contrast, the energy barrier is 2.15 eV on the oxygen vacancy-free CeO_2. The abundant surface defects and large surface area of CeO_2 can provide sufficient surface-active sites and thereby deliver apparent peroxidase-like activity.

Thus, both experimental and theoretical investigations suggest that the relatively low levels of structural defects of previously reported CeO_2 nanomaterials cause the unconspicuous peroxidase-like activity. Afterwards, various methods have been explored to increase the abundance of structural defects of CeO_2-based catalysts and enhance their peroxidase-like activity. The Co-doped mesoporous cerium oxide has been reported to exhibit two order of magnitude enhancement in the biomimic peroxidase-like catalytic efficiency than that of mesoporous nanoceria alone under the near-neutral environment [98]. The hollow mesoporous Mn/Zr-co-doped CeO_2 synthesized by a facile wet chemistry approach via Kirkendall effect introduced Zr^{4+} and Mn^{2+} into the lattice of CeO_2 and thereafter significantly increased the

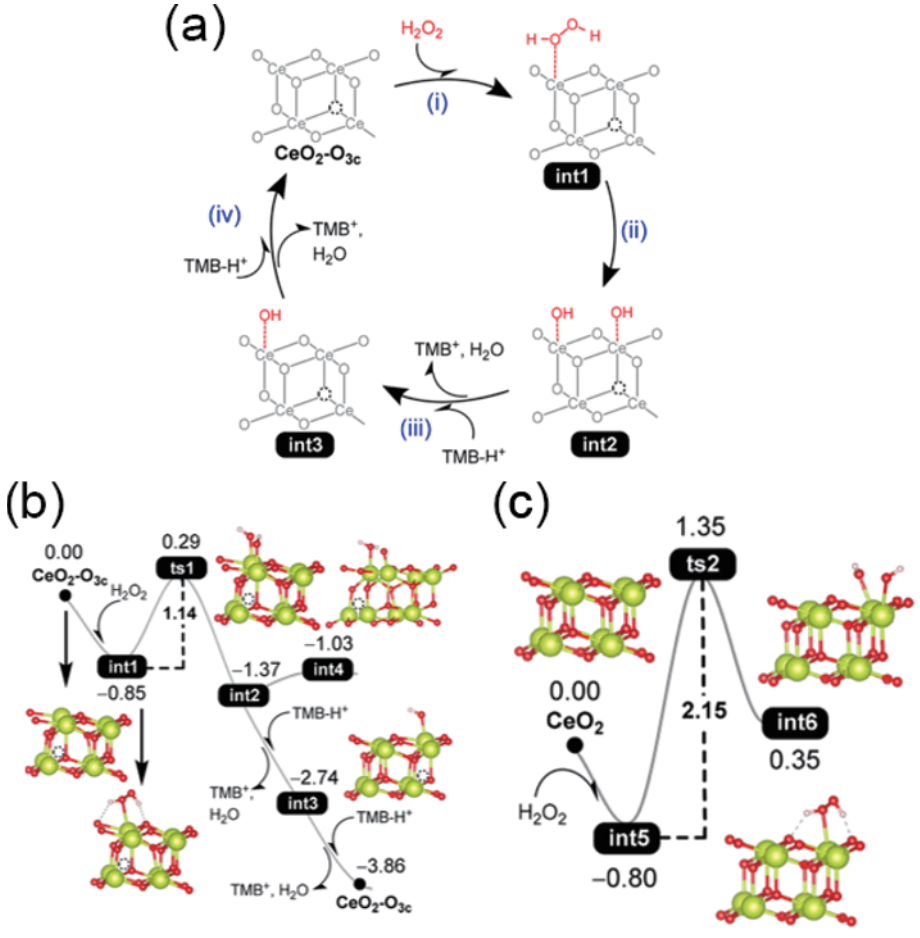

Figure 4 DFT simulations on the catalytic mechanism of peroxidase-mimicking activity of CeO_2 catalysts. (a) Proposed catalytic mechanism. (b) Reaction energy profile for the defective CeO_{2-x}. (c) Energies for the decomposition of H_2O_2 on ideal CeO_2 without oxygen vacancy. The energy unit is eV. Reproduced with permission from Ref. [97], © American Chemical Society 2021.

peroxidase-like activity in comparison with CeO_2 alone in a mildly acidic environment. The improved performance is primarily ascribed to the accelerated redox cycles from Ce^{4+} to Ce^{3+} via the intermetallic charge transfer due to the chemical doping of Mn^{n+} with variable chemical states [99]. Besides, metal-doped nanoceria exhibits stronger H_2O_2 adsorption strengths than pure ceria, showing the enhanced peroxidase-mimetic activity [98]. Finally, the dramatically elevated ratio of Ce^{3+}/Ce^{4+} of the Cu-doped CeO_2 nanozyme induced a significant improvement of peroxidase-like activity in the weakly acidic pH media [100].

Despite those progresses, the proposed catalytic mechanism is still highly controversy due to the stability of oxygen vacancy of CeO_2 nanozymes. A recent study suggested that the generated oxygen vacancy by heteroatom doping or other physical treatments was unstable in the water at ambient conditions due to the water replenishment, leading to an enhanced level of the interfacial hydroxyls [101]. Thus, those oxygen vacancies were suspected that they are not the active sites for the H_2O_2 activation in aqueous environment. While, the metastable oxygen vacancy of CeO_2 has been reported to be water-resistant [102]. Peng et al. employed theoretical calculations to analyze the surface electronic structure of different CeO_2 facets. Three types of metastable oxygen vacancy with different local structures and chemical states are formed on CeO_2 (111), (110), and (100) surfaces: seven-coordinated Ce atom with one vacant orbital on Ce(111); six-coordinated Ce atom with two vacant orbitals but different electronic configurations on (110) and (100) surfaces (Fig. 5(a)) [96]. Thus, the local structures and chemical states play important roles for the H_2O_2 activation in physiological environment. The electron density of the surface Ce species was in the order of (100) > (110) > (111) due to the local surface reconstruction and thereafter changed coordination environments of different facets, which was also demonstrated by XPS and ^{31}P NMR by using trimethylphosphine as probe molecule. The strong adsorption of H_2O_2 on the metastable oxygen vacancy of CeO_2 may not guarantee its effective activation. Various characterizations and DFT calculations suggested that CeO_2 (100) surface with six-coordinated Ce atom as well as the high electron density promoted the H_2O_2 adsorption and activation with a lower kinetic energy barrier and easily recovered the metastable oxygen vacancy for next catalytic reaction, thereby improving the peroxidase-like activity of CeO_2 nanozymes. Based on those, CeO_2 cubes enclosed by (100) facet were experimentally demonstrated to deliver a very impressively high peroxidase-like activity, which was 211.8 and 35.8 times higher than CeO_2 octahedrons and nanorods (Fig. 5(b)) [96, 101].

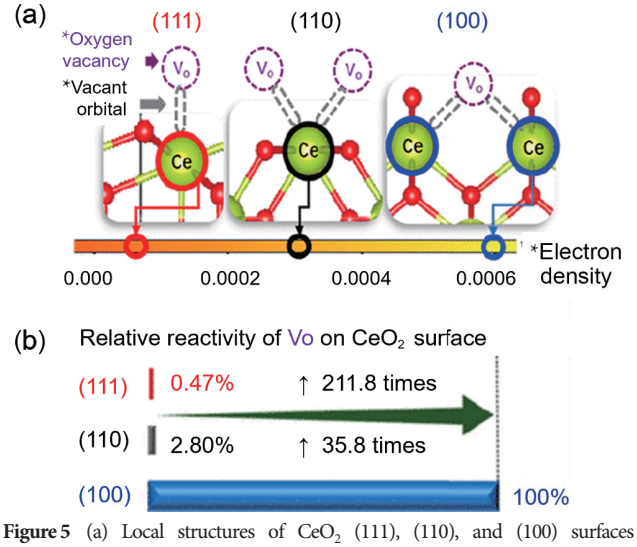

Figure 5 (a) Local structures of CeO_2 (111), (110), and (100) surfaces including the coordination number of surface Ce, the direction/number of vacant orbitals, and the metastable oxygen vacancy. (b) Comparison of catalytic activity of CeO_2 nanozymes of cubes, rods, and octahedrons as peroxidase mimics. Reproduced with permission from Ref. [96], © The Royal Society of Chemistry 2020.

3.2 Oxidase-like activity

Unlikingly peroxidases with H_2O_2 as electron acceptor to generate reactive oxygen species, oxidases, a family of natural enzyme, catalytically activate molecular O_2 to produce active oxygen species and oxidize target substrates. The dextran-coated CeO_2 nanoparticles were the first example of CeO_2 nanozyme to deliver the oxidase-like activity for oxidation of various colorimetric substates including TMB, dopamine (DOPA), and 2,2-azino-bis(3-ethylbenzothizoline-6-sulfonic acid) (AzBTS) in acidic conditions (Fig. 6(a)) [34]. The best catalytic oxidase-like activity of nanozymes was found in the acidic media with pH 4.0. The evidence for this oxidase-like activity of dextran-coated CeO_2 instead of peroxidase-like behavior was attributed to high activity in the absence of H_2O_2 and decayed activity in the absence of O_2. Various control experiments suggested the dextran-coated CeO_2 with a smaller size and a thinner polymer layer delivered a higher catalytic oxidase-like activity in media with a lower pH value. A thinner surface polymer layer can promote the diffusion of substrate into the surface-active sites of CeO_2 nanozymes. Small-sized CeO_2 can introduce more surface oxygen vacancy and provide more active sites for oxidation. Besides those, the types of polymers also significantly affect the oxidase-like activity of CeO_2. When the same CeO_2 nanoparticles were used, poly(acrylic acid)-coated CeO_2 exhibited 2-fold higher catalytic activity than that of dextran-modified CeO_2. While, poly(sodium acrylate) and poly(ethylene glycol) as the coating layers impair the oxidase-like activity of CeO_2 nanozymes [103].

Our recent studies indicated that the oxidase-like activity of poly(styrene sulfonate) (PSS)-coated PN-CeO_2 displayed a volcanic-like behavior as the function of the molecular weights of PSS (Fig. 6(b)) [43]. In this configuration, the hydrated PN-CeO_2-PSS catalysts with large hydrodynamic diameters formed a nanoreactor to confine and capture more O_2 molecules and targeted substrates, improving the capability for the catalytic generation of O_2^- species and enhancing activity for TMB oxidation inside of nanoreactors afterwards (Fig. 6(c)). The catalysts exhibited an apparent pH-activity dependence with a very high catalytic activity in acidic conditions (pH < 5.0), a quite good catalytic performance in weakly acidic medias (5.0 < pH < 7.0) and a barely oxidative capability under normal physiological environments (pH 7.4) and in alkaline environments. The nanozymes with the greatly enhanced oxidase-like activity under O_2 and the inhibited activity under Ar suggested O_2 as electron acceptor to generate ROS for the oxidative reaction. The volcanic-like performance of PN-CeO_2-PSS was attributed to their hydrodynamic diameter. Generally, a too-large hydrodynamic diameter of the nanozymes is generally observed on PSS with larger average molecular weight. Despite trapping more O_2 and reactants inside the constructed nanoreactors with large molecular weights of PSS, the decreased charge transfer between the hybrids and reactants results in a decayed activity (Fig. 6(d)). The smaller hydrodynamic diameter of PN-CeO_2-PSS with small molecular weight of PSS produces a smaller nanoreactor, leading to less amount of trapped O_2 and reactants and thereby exhibiting a lower oxidase-like activity. The balance of the charge transfer between nanozymes and reactants and the confinement effects of nanoreactors for enrichening reactants determine the volcano-like hydrodynamic diameter–activity correlation of various PN-CeO_2-PSS catalysts.

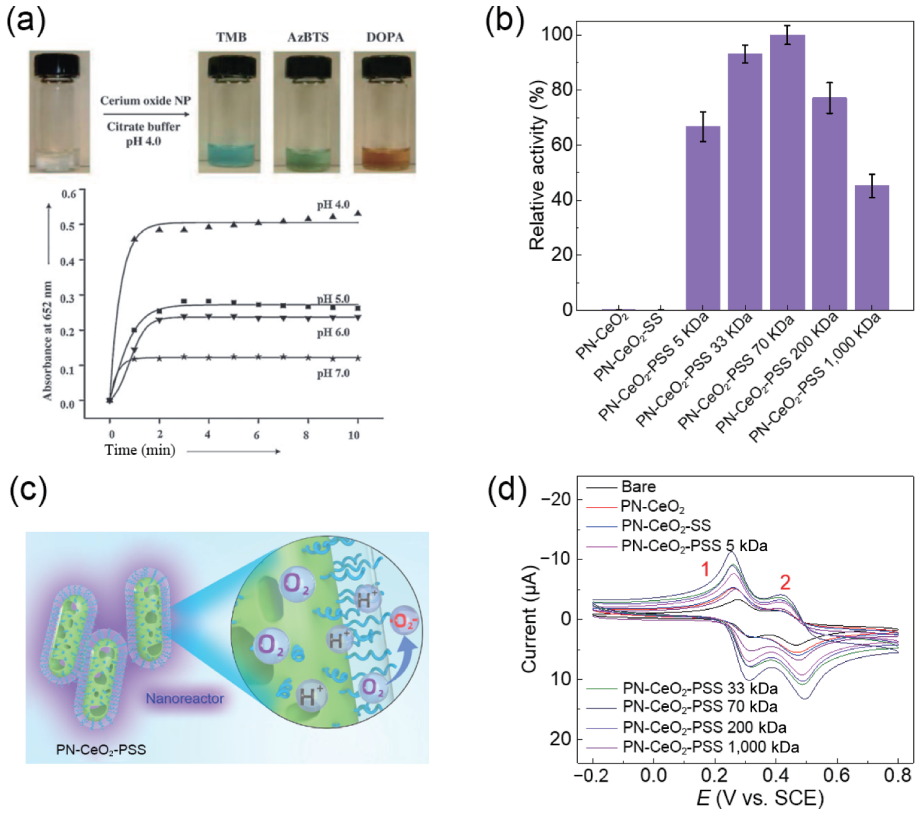

Figure 6 CeO_2 nanozymes as oxidase mimics. (a) Catalytic performance of the dextran-coated CeO_2. Reproduced with permission from Ref. [34], © WILEY-VCH Verlag GmbH & Co. KGaA, Weinheim 2009. (b) Volcanic-shaped correlation of catalytically oxidative activity of PN-CeO_2-PSS as a function of molecular weight of PSS. (c) Proposed mechanism of PN-CeO_2-PSS as artificial oxidase. (d) Charge transfer as a function of molecular weight of PSS. Reproduced with permission from Ref. [43], © Wiley-VCH GmbH 2020.

Besides the polymer encapsulation, the F^- ions modification also significantly enhanced the catalytic activity of CeO_2 nanoparticles as oxidase mimics by a factor of ~ 100 [104]. It could be attributed to the modulated surface charge of CeO_2 nanozymes from positive charge to negative charge, when the concentration of F^- ions was over 5 mM. Then, it would benefit the adsorption of reactants and the desorption of the generated products, when AzBTS and TMB were used as the substrates. Besides the change of surface charge, the spectroscopic studies also indicated that F^- replaced the surface hydroxyl groups and effectively increased the surface Ce^{3+} fractions, contributing to the improved catalytic oxidative activity of the modified CeO_2 nanozymes as well.

3.3 Superoxide dismutase-like activity

Apart from the catalytic generation of ROS by CeO_2 nanozymes with H_2O_2 or O_2 as electron acceptor, CeO_2 is widely explored as artificial nanozymes to deliver the SOD-like activity for the ROS degradation in the biological systems [40, 42, 55, 67, 105–107]. The SOD-like performance of ceria nanostructures is also considered to be originated from the switchable Ce^{3+}/Ce^{4+} redox pair, as shown in Fig. 7(a) [67]. In this proposed catalytic pathway, the capability of the valence switch ability between $Ce^{3+} \leftrightarrow Ce^{4+}$ makes CeO_2 to deliver SOD-like activity and exhibit antioxidant behavior by degrading ROS into harmless chemicals.

Generally, the defective CeO_2 catalysts with abundant surface Ce^{3+} species exhibited a high SOD-like capability for ROS degradation [40, 42, 55, 67, 105–107]. However, the surface properties (surface defect levels, chemical composition, exposed facets, surface capping reagents, etc.) of various CeO_2 catalysts have not been quantitatively accounted for their SOD-like performance in early investigations. Thus, the evaluations on their apparent SOD-like activity might not reflect the quantitative relationships between the surface physicochemical properties and the intrinsic activity of ceria nanozymes. According to previous mechanism studies, each surface Ce^{3+} site can be considered as an active center for mimic SOD. Normalizing the activity to each Ce^{3+} specie with the consideration of surface areas of various catalysts can provide the quantitative relationship between the surface properties of CeO_2 catalysts and their capability for eliminating ROS. By comparing the normalized catalytic activity of CeO_2 nanorods, CeO_2 nanoparticles, and PN-CeO_2, the higher activity of PN-CeO_2 and nanorods was ascribed to the dominated (100) and (110) facets of those two nanozymes (Fig. 7(b)) [42]. Ultrathin walls of PN-CeO_2 introduced the presence of low-coordinated surface cerium species and thereby resulted in higher intrinsic activity of PN-CeO_2 over nanorods. When PN-CeO_2 was used as model catalysts and their surface amounts of Ce^{3+} species were modulated through thermal treatments without morphological changes, the normalized catalytic activity was almost identical for all PN-CeO_2 catalysts (Fig. 7(c)). Thus, the morphologies of CeO_2 nanozymes also influence their catalytic performance as SOD mimics, which is attributed to the different formation energy of oxygen vacancy on each exposed crystal plane of ceria catalysts. However, the intrinsic SOD activity of each Ce^{3+} site on the well-defined facet is near constant no matter what sizes and abundances of oxygen vacancy of CeO_2 catalysts [42].

A recent investigation also suggested that the catalytic performance of CeO_2 as biomimic SOD catalysts showed a strong correlation with the Ce^{3+} surface area concentration ($c_S f_{Ce^{3+}}$), in which CeO_2 nanoparticles with various sizes were used catalysts. The c_S is described by $A_S c$ with A_S as the specific surface area of ceria and c as the weight concentration of ceria nanozymes in solution. The $f_{Ce^{3+}}$ represents the fraction of Ce^{3+} species of CeO_2 naozymes. Generally, the larger value of $c_S f_{Ce^{3+}}$ indicates the higher SOD-like activity of CeO_2 catalysts. The single profile of the

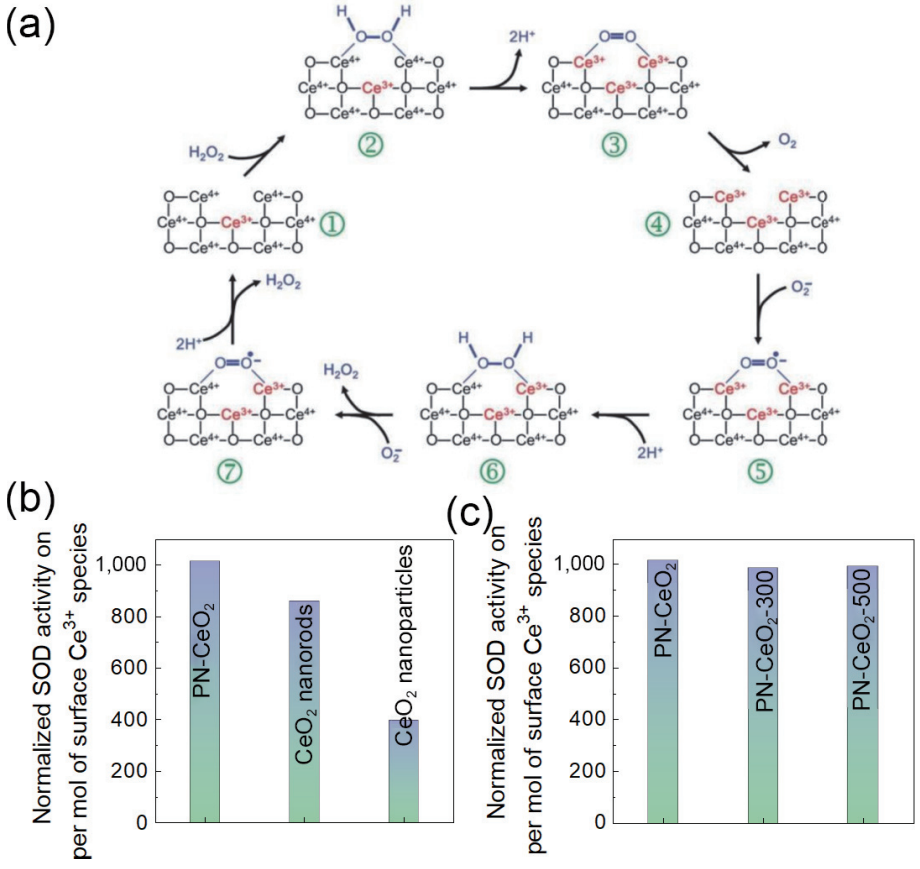

Figure 7 (a) Proposed catalytic mechanism of CeO_2 as SOD mimetics. Reproduced with permission from Ref. [67], © The Royal Society of Chemistry 2011. (b) The normalized SOD activity on the total amount of the surface Ce^{3+} species for PN-CeO_2, and CeO_2 nanorods and nanoparticles. (c) The normalized SOD activity on the total amount of the surface Ce^{3+} species for as-synthesized PN-CeO_2 and the thermally treated PN-CeO_2 in air under 300 and 500 °C. Reproduced with permission from Ref. [42], © American Chemical Society 2017.

catalytic activity functioned with the $cs f_{Ce^{3+}}$ also suggests a particle independent redox mechanism, when the same shaped CeO_2 nanozymes were used [39].

A recent theoretical investigation proposed that the *in-situ* created transition surface defect states instead of Ce^{3+}/Ce^{4+} ratio could be used as a better parameter to evaluate the SOD-like capability of various defective ceria catalysts [108]. This study raised this concern due to the experimentally inaccurate determination of the defect concentration of CeO_2 catalysts by XPS technique in some specific cases. Transition surface defect states (SDS) described the newly generated SDS in the electronic band structures of the transient intermediates on catalyst surface. Each oxygen vacancy can introduce two SDS in the electronic band structures of ceria catalysts, which correspond to the surface Ce^{3+} species. In comparison with the high mobility of oxygen vacancy and thereby unsettling locations of the Ce^{3+} species in crystal lattice, the energy of the created SDS strongly correlates with the reducibility of the defective CeO_2 nanozymes. Generally, the higher reducibility of CeO_2 introduces the better SOD-like activity with a higher O_2^- scavenging capability. How to determine the surface defect states is still experimentally challenging.

3.4 Catalase-like activity

Catalase is natural enzyme, which catalytically converts oxidative H_2O_2 into harmless O_2 and H_2O. CeO_2 has been widely explored as the artificial catalase for the reversible Ce^{3+}/Ce^{4+} redox pair [55, 67, 109–113]. This reaction is generally adopted with a multiple-step process (Fig. 8): (1) adsorption and activation of H_2O_2 on two Ce^{4+} sites; (2) deprotonation for release of two H^+; (3) reduction of Ce^{4+} species on CeO_2 surface to give a molecular O_2 and surface Ce^{3+} species; (4) adsorption and activation of H_2O_2 on two newly formed Ce^{3+}; (5) uptake of two proton with the oxidation of two Ce^{3+} species; and (6) release of two H_2O and restore of the surface Ce^{4+} sites for the next catalytic reactions [67]. The catalytic mechanism suggests that the surface Ce^{4+} site initiates the catalytic reaction. Thus, the highly defective or reduced CeO_2 has been reported to deliver a low catalase-like activity. Additionally, an exhaustive molecular mechanism for CeO_2 as artificial catalase suggested the existence of the chemical reduction approach. Thus, CeO_2 as a reductant instead of a catalyst is proposed. Therefore, further efforts are expected to provide the insightful understandings on catalytic mechanisms of nanoceria as the artificial oxidase catalysts with high performance.

3.5 Photolyase-like activity

DNA photolyases are a family of natural enzymes that catalytically reverse the ultraviolet (UV)-induced cyclobutene pyrimidine dimers (CPD) between two adjacent thymines in a DNA strand and thereby repair DNA damage [61, 114–117]. UV-induced formation of CPD is detrimental to human skins, which potentially induces many serious skin diseases and even leads to skin cancers. Photolyases can catalytically repair such a UV-reduced DNA damage through a photocatalytic process under the irradiation of the blue light (Fig. 9(a)) [61, 114]. The transfer of the photogenerated electrons into the four-member ring can break the intradimer bonds and restore the original sequence of DNA (Fig. 9(b)) [115, 116]. DNA photolyases found in many plants and animals, unfortunately, do not exist in human skin. Principally, this repair process is highly analogy to a photocatalytic process enabled by semiconductors (Fig. 9(c)), giving opportunities to design photocatalysts as the artificial nanozymes to mimic the natural photolyases by taking advantage of photoelectrons [116,

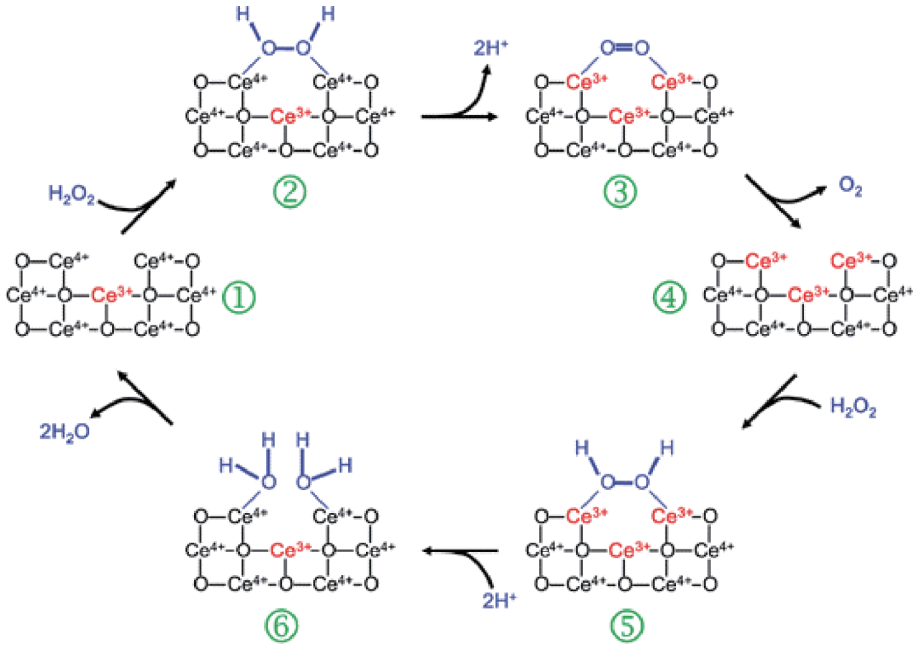

Figure 8 Proposed catalytic mechanism of CeO_2 as catalase mimetics. Reproduced with permission from Ref. [67], © The Royal Society of Chemistry 2011.

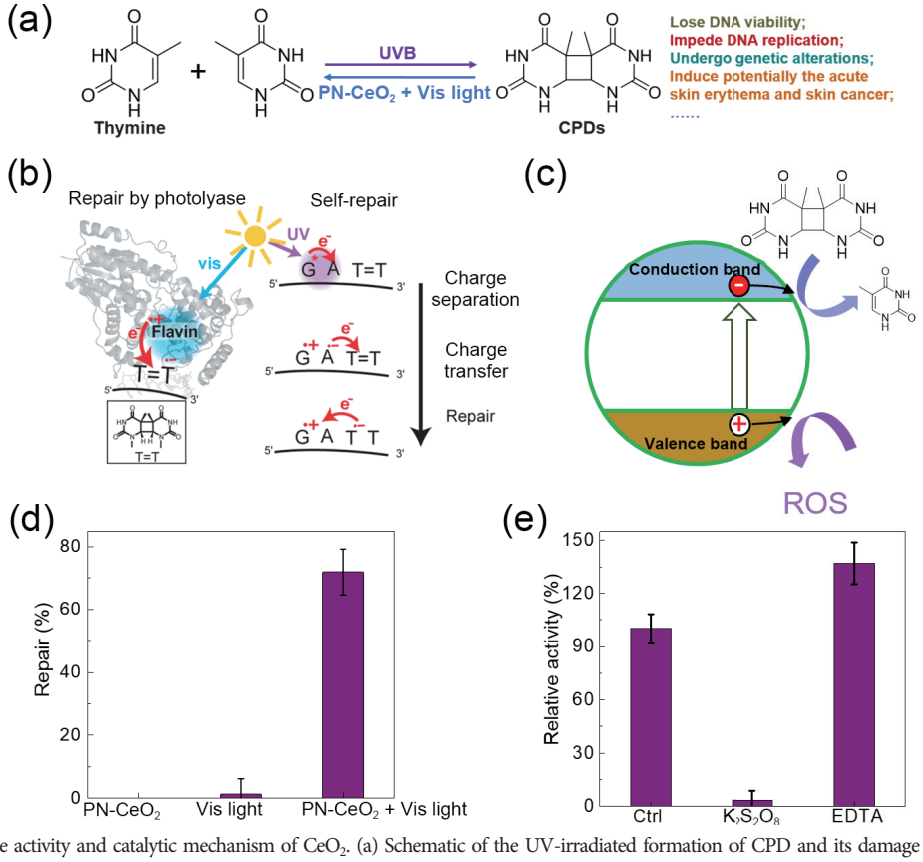

Figure 9 Photolyase-like activity and catalytic mechanism of CeO_2. (a) Schematic of the UV-irradiated formation of CPD and its damage as well as the repair. (b) Catalytic mechanism of natural photolyases. Reproduced from Ref. [116], © American Chemical Society 2015. (c) Photocatalytic process of semiconductors and its similarity with natural photolyase. (d) Photolyase-like performance of PN-CeO_2 under various conditions. (e) Catalytic performance of PN-CeO_2 in presence of electron and hole scavengers. Reproduced with permission from Ref. [61], © American Chemical Society 2019.

117]. However, majority of semiconductors cannot serve as artificial photolyases due to the photo-generation of highly oxidative ROS, which can induce the decomposition of CPDs into fragments. Different from other semiconductor, CeO_2 delivers its potential to deliver the photolyase-like activity due to its semiconductor nature for generation of photoelectrons as well as its SOD-like activity for local degradation of the photo-generated ROS [55, 67, 107].

As confirmed from liquid chromatography-mass spectrometer, PN-CeO_2 delivered the photolyase-like activity, which successfully enabled a selective cleavage of dimer into monomers (Fig. 9(d)) [61]. While, negligible amount of CPDs was restored without visible light or nanozymes, revealing the intrinsic activity of PN-CeO_2 as artificial photolyase for DNA repair. The significantly promoted activity with addition of ethylenediaminetetraacetic acid (EDTA) as the hole scavenger and its poor activity in the presence of $K_2S_2O_8$ as the electron scavenger demonstrated a photocatalytic process enabled by porous nanorods of ceria, analogy to that of

natural photolyase enzymes (Fig. 9(e)). Mechanism investigations indicated a high level of structural defects of oxygen vacancy (indexed by surface Ce^{3+} fraction) and porous structures as the key factors to activate the catalytic capability of PN-CeO_2 as artificial photolyase. Abundant surface defects not only enhance the light absorption of ceria nanozymes within the visible light range, but also improve the affinity of substrates with the catalysts as revealed from the fitted catalytic data K_m by the Michaelis–Menten equation. The porous structures further enhance the interaction between substrates and catalysts and improve the transfer of the photo-generated electrons through capillary effects. Thus, the highly defective PN-CeO_2 shows its promising potentials as a stable and effective inorganic anti-UV reagents for the protection of human skins, which might be extended as candidates to mimic other natural photo-enzymes.

3.6 Phosphatase-like activity

Phosphatases are natural enzymes that cleave phosphate groups from phosphoric acid esters through a hydrolytic process. High activity and substrate selectivity make phosphatases as essential enzymes for many phosphorous metabolisms. Thus, they have been widely used for the enzyme-linked immunosorbent assays. CeO_2 has been found to possess the phosphatase-like activity due to its highly defective nature at nanoscale with the abundant Ce^{3+}, Ce^{4+} species, and oxygen vacancy sites for the adsorption of phosphate groups, activation of water, and subsequent hydrolysis [55, 60, 95, 118, 119]. Despite the wide report of the phosphatase-like activity, the catalytic mechanism of CeO_2 nanozymes is still controversial, as showed in previous reports with different interpretations and even disagreements.

Generally, the interfacial Ce^{4+} cations as the Lewis acidic sites are coordinated by phosphate group of substrates. While, the interfacial Ce^{3+} cations serve as active sites for water adsorption and activation to generate the surface hydroxyl species. Due to the strong electron-withdrawing capability of Ce^{4+}, the reduced electron density of P makes it easier for a nucleophilic attack by the surface hydroxyl. Followed by this mechanism, due to the short P–O bond, the interfacial hydrolysis has to be guaranteed by the proper spatial arrangement of Ce^{4+}, Ce^{3+}, and oxygen vacancy. While, the phosphatases-like activity of CeO_2 was also reported to depend on interfacial Ce^{3+} species and to be suppressed by Ce^{4+} species [120].

From majority of previous investigations, the adsorption of phosphate groups on the Lewis acidic sites of CeO_2 is critical for the P=O bond activation and consequential hydrolysis. While, the strong adsorption of phosphate group or the generated phosphate ions (PO_4^{3-}) on CeO_2 catalysts generally induces a self-limited catalytic performance. A recent DFT calculation with CeO_2 (111) as a model surface suggested that the desorption of phosphate group from catalyst surface instead of the P=O bond activation was rate-determined step [121]. Therefore, the recovery of the interfacial catalytic centers of CeO_2 became difficult. Thus, some investigations suggested the non-catalytic process of this pephosphorylation catalyzed by CeO_2 nanozymes, when the strongly adsorbed phosphate groups occupy the interfacial active sites of ceria catalysts [119]. Meanwhile, the rapidly reversible Ce^{3+}/Ce^{4+} cycle and a high oxygen mobility of CeO_2 have been reported to dynamically create phosphatase-mimetic activity and regenerate the surface-active sites. Overall, the mechanism of phosphatase-like activity of CeO_2 under high debate [122].

Besides those arguments, the CeO_2 nanocubes generally showed the bare activity for dephosphorylation reaction at room temperature, indicating that the Ce^{4+} species on the surface of CeO_2 (100) are inactive without rational explanation. It indicates the Ce^{3+}/Ce^{4+} fraction derived from XPS might not give the very accurate information of chemical states of CeO_2. Since the different formation energy of oxygen vacancy on each crystal plane of CeO_2, the chemical states of cerium ions in terms of electron density as well as their Lewis acidity would be greatly different on each exposed facet. Thus, the adsorption/activation energy of P=O bond would vary from facet to facet, causing the acidity of CeO_2 might be used as the key factor to control phosphatase-like activity of CeO_2. Peng's group used the ^{31}P NMR with trimethylphosphine (TMP) as a probe molecule to distinguish and quantify the chemical states or acidity of the interfacial Ce species of various shaped CeO_2 catalysts including nanorods (enclosed by (110) and (100) facets), cubes (enclosed by (100) facet), octahedrons (enclosed by (111) facet), and sphere nanoparticles with mixed facets [36, 95]. As reflected from δ ^{31}P of trimethylphosphine oxide adsorbed CeO_2 (TMPO-CeO_2) nanozymes (Fig. 10(a)), a morphology-dependent order of the Ce chemical state was observed: 50.2 ppm (octahedron) > 47.2 ppm (rod) > 45.1 ppm (cube). The NMR results suggested the stronger Lewis acidity on the CeO_2 (111) and lower Lewis acidity on the CeO_2 (100). Thus, the more Ce^{4+} species are found on CeO_2 (111) surface. Also, the CeO_2 (100) surface is dominated by Ce^{3+}. Using p-nitrophenyl disodium orthophosphate (p-NPP) as reactant, various CeO_2 nanozymes as phosphatase mimics delivered the catalytic activity with an order of octahedron, nanorod, and cube, which was consistent with the Lewis acidity of interfacial Ce species on the main terminal facets.

Derived from NMR peaks, the $[Ce]_{surface}$ (surface Ce density normalized by catalyst' weight, μmol/g) at a specific acidity was quantitated in an order of 0.61 (octahedra) > 0.37 (rod) > 0.21 (cube) (Fig. 10(b)). When the amount of CeO_2 cubes was increased by a factor of 2 or 3, the catalysts still did not exhibit the apparent phosphatase-like activity at room temperature, suggesting that acidity of Ce species on CeO_2 (100) surface was not high enough to activate this reaction. The correlation between Ce acidity and the activation energy/reaction constant k_c of various defective ceria catalysts further demonstrated that decreasing the acidity of surface Ce species reduced the Ce specific activity and hence lowered the phosphatase-like activity of ceria catalysts. Thus, the threshold of Ce acidity to efficiently activate P=O bond at room temperature is over that of CeO_2 cubes (45.1). As a summary, Fig. 10(c) illustrates the relationship between the acidity of interfacial Ce of ceria catalysts and their activation for catalytic dephosphorylation.

3.7 Haloperoxidase-like activity of CeO_2

Haloperoxidases, a family of enzymes, catalytically oxidize halides (X = Cl^-, Br^-, and I^-) by H_2O_2 into the reactive hypohalous acid (HOX) species. As intermediates, HOX can halogenate the N-acylhomoserine lactones, which are the important signaling molecules in bacterial quorum sensing [123]. Thus, the haloperoxidase can serve as the effective component of antifouling layers, especially for those against adhesions of marine microorganisms on the surface of marine equipment under the marine conditions [62, 123–126].

Inspired the rapid Ce^{3+}/Ce^{4+} redox cycle and the capability of the interfacial Ce^{3+} sites for the activation of H_2O_2, CeO_2 has been demonstrated as the efficient heterogeneous catalysts for the halogenation of malonic acid. Afterwards, CeO_2 nanorods have been experimentally examined to deliver haloperoxidases-like activity for combating biofouling in the mimetic marine conditions. Catalytic mechanism investigations showed that the interfacial Ce^{3+} sites serve as active sites to be occupied by H_2O_2 and then activate it (Fig. 11) [62]. DFT calculations suggest that the generation and release of reactive oxygen species are a slow process. In contrast, the direct addition of halides to one of oxygen

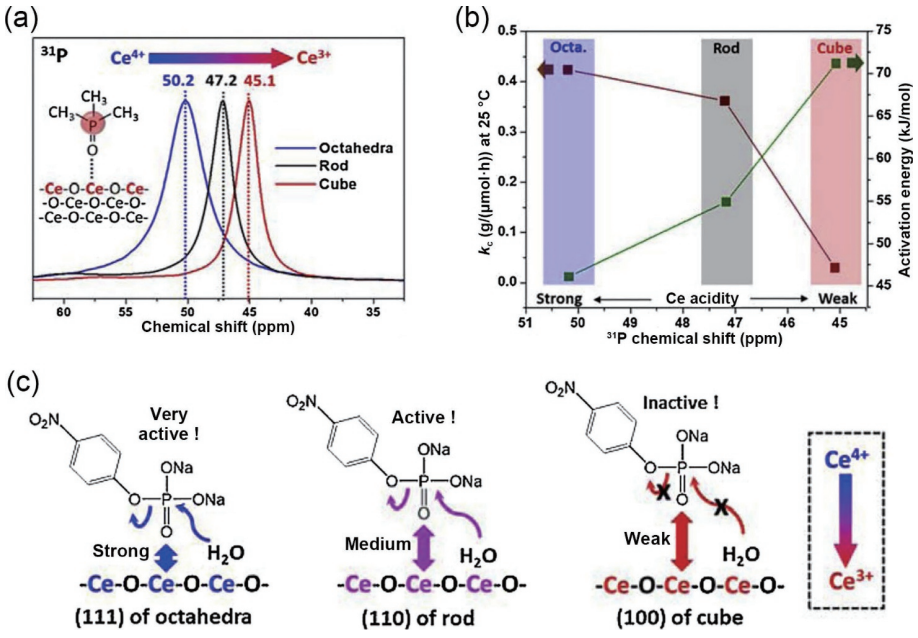

Figure 10 (a) ^{31}P NMR spectra of TMPO-adsorbed CeO_2 catalysts with different shapes. (b) Correlation of Ce acidity of various shaped CeO_2 nanozymes and their catalytic performance. Reproduced with permission from Ref. [36], © American Chemical Society 2020. (c) Schematic illustration of the acidity-depended phosphatases-like activity of various shaped CeO_2 nanozymes. Reproduced with permission from Ref. [95], © Elsevier B.V. 2019.

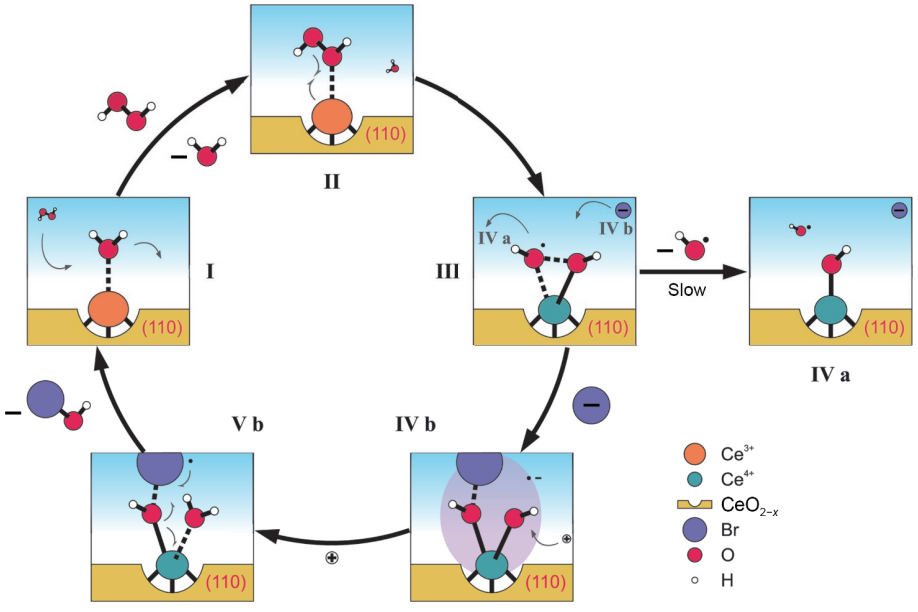

Figure 11 Proposed catalytic mechanism of the defective CeO_{2-x} nanorods for bromination. Reproduced with permission from Ref. [62], © WILEY-VCH Verlag GmbH & Co. KGaA, Weinheim 2016.

atom of the adsorbed H_2O_2 to form the interfacial intermediate of HOX and one hydroxide ligand is energetically favorable pathway. The hydroxide is protonated to give a neutral surface site. With the release of HOX, the water-adsorbed Ce^{3+} active site is restored for next reaction. Therefore, CeO_2 with the large surface area and high level of structural defects provides the abundant surface Ce^{3+}speices and thereafter brings a higher haloperoxidases-like activity.

Following this understanding on catalytic mechanism, CeO_2 nanotubes synthesized through chemical etching of CeO_2 nanorods delivered high haloperoxidases-like activity for a large surface area and a slightly high structural defects of nanotubes [44]. Bi-doped CeO_2 nanozymes delivered a three-fold enhancement for the generation of HOBr over CeO_2 nanorods under the equal conditions, which was attributed to the enhanced ζ-potential of surface-engineered Bi-doped CeO_2 nanoparticles and subsequently facilitated adsorption of the halides on catalyst surface in aqueous environments [124]. Although this study did not provide the information of structural defects, the enhanced abundance of oxygen vacancy and interfacial Ce^{3+} due to the Bi-doping might also contribute the improved catalytic haloperoxidases-like activity. Fabrication of CeO_2 nanorods embedded in the polyvinyl alcohol through electro-spinning method enhanced the wettability of nanozymes and improved mechanical stability of hybrids, leading to the increased haloperoxidases-like activity and stability to produce HOBr for combating bacterial adhesion [125].

3.8 Other enzyme-like activity of CeO_2

Besides those enzyme-like activities, CeO_2 with the advantages of low cost, good biocompatibility, and long-term stability also exhibits the ability to strongly adsorb nucleotides and DNA. Similar to the capability of CeO_2 with phosphatase-like activity, the defective CeO_2 nanoparticles could offer DNase I mimic activity

for the hydrolytic cleavage of DNA oligonucleotides [127]. Ureases are a family of metallohydrolases that catalyze the hydrolysis of urea (an important molecule in medical and environmental analysis) into ammonia and carbon dioxide. CeO_{2-x} nanorods have been demonstrated to present an intrinsic urease-like activity, which catalyzed the hydrolysis of urea under ambient conditions. Derived from Michaelis–Menten equation, the urease-like catalytic activity (K_{cat}) of CeO_{2-x} nanorods was estimated to be 95.8 s^{-1}, which was one order of magnitude lower than that of the native jack bean urease [128]. Also, CeO_{2-x} nanorods also exhibited a stable urease-like activity against pH changes.

4 Summary and perspective

The developments of nanozyme aim to use nanomaterials to replace nature enzymes. The mechanism of a nanozyme is related more to heterogeneous catalysis in terms of the reaction process. The present understandings of the enzyme-like mechanisms of CeO_2 catalysts are primarily attributed to the highly reversible redox Ce^{3+}/Ce^{4+} pair under ambient conditions, which shows a high similarity to the catalytic processes of natural enzymes. Majority of investigations on the catalytic mechanisms generally ignore the dynamically structural evolutions and real surface chemical states of CeO_2-based nanozymes during the practical catalytic reactions. Thus, it even leads to the contradictory viewpoints on the same reaction catalyzed by the same type of catalysts. To comprehensively investigate catalytic mechanisms by taking the real-time surface structures and electronic configurations of CeO_2-based nanozymes into accounts can offer insightful comprehension. Improved understandings on the catalytic mechanism of nanozymes at molecular and electronic levels will in turn benefit the design and synthesis of novel nanozymes with high activity and specificity, which will enable the practical applications for the clinic diagnosis and disease treatments. Herein, we concentrated on the recent advances on the explorations of catalytic mechanisms of CeO_2-based catalysts as artificial enzymes. Academic fundamental investigations on the catalytic mechanism can pave the ways for the practical applications of those nanozymes, including the highly sensitive biosensor and the safe therapeutic strategy for neurodegenerative diseases, cardiovascular, inflammation, and tumor therapy. So far, the catalytic performance of CeO_2-based nanozymes is still severely limited by their unsatisfied activity and poor specificity. Generally, the multiple enzyme-like performances of CeO_2 are found, which depend on the surface microenvironments as well as the catalytic conditions. For instance, the nanoceria catalysts provide high capability against tumors; meanwhile they also protect the normal organs from negative effects of chemotherapy drug [42, 43, 59]. Besides, explorations of the phosphatase-like, haloperoxidases-like, and urease-like activity of nanoceria may also open promising avenues for the therapeutic activity of CeO_2. Overall, considering the enormous potentials of CeO_2-based nanozymes and substantial opportunities in this area, there remain more challenges on the catalytic mechanism for the further improvement of their activity and specificity.

(1) The identification of active sites of CeO_2-based nanozymes is prerequisite for the further improved activity and specificity. The enzyme-like performance of ceria is largely determined by the structural defects of oxygen vacancy. Both the geometry and abundance of structural defects can modulate the spatial configurations and electronic structures of the interfacial catalytic centers of CeO_2 nanozymes. Since the high mobility of oxygen vacancy in CeO_2 lattice and the possible structural reconstruction of ceria catalysts under the practical operation, it makes difficulty in capturing the exact the active sites on the catalyst surface. Although various techniques including XPS, NMR, XAS, Raman, and FTIR can provide the surface information, majority of investigations focused on characterizations on as-synthesized and/or the spent catalysts, leaving the unknown surface states of the catalysts during catalytic reactions. Also, the state-of-the-art studies on the surface properties of CeO_2 rely on one or few surface techniques, which might not provide the overall and very accurate structural and surface physicochemical properties. Thus, the developments of new techniques and methodology to *in-situ* monitor the surface evolution of CeO_2 catalysts are highly anticipated.

(2) The controllability of catalytic activity and specificity of CeO_2-based nanozymes is highly desired for practical applications. Principally, a high activity of CeO_2 nanozymes as the active components for sensors is expected to lower the limit of detection. Meanwhile, a high catalytic selectivity is pivotal for the accuracy of analytical results by excluding various interferences from environments. For *in vivo* biomedical applications, the catalytic activity of nanozymes has to be tailored at certain level for the increase or decrease of the target species under the physiological environments since they serve as the important message molecules/species. Too high activity or too low activity of nanozymes might not realize the catalytic purposes under *in vivo* conditions. While, the catalytic selectivity of CeO_2 nanozymes has to be further improved under the physiological environments for both normal organs or local lesions. Due to the multiple enzyme-like activity driven by the reversible Ce^{3+}/Ce^{4+} redox pair, catalytic specificity of ceria nanozymes has not well explored under the environments of the practical applications. Further explorations on both activity and specificity in application scenarios are critical for the practical applications of CeO_2 nanozymes.

(3) The quantification of activity of CeO_2 nanozymes is important for the evaluation of enzyme-like activity. Unlike the natural enzymes with the identified method to characterize their catalytic activity by being normalized to each active center, the dynamic surface of CeO_2 nanozymes makes it impossible to account the exact number of surface active sites. Standardizing their activity on mass, surface area, or surface Ce^{3+} fractions is not accurate since there are too many factors to influence the catalytic behaviors of CeO_2 catalysts. Analogy to the heterogeneous catalysis, accounting the total active sites might be suitable for nanozymes. Again, how to reach a general measurement or calculations on active sites of CeO_2 is still lack due to the dynamic changes of CeO_2 surface and high oxygen mobility.

(4) The influences of the adsorbed small molecules and ions on the catalytic activity and specificity should be considered for CeO_2-based nanozymes in both experimental and theoretical investigations. Generally, the CeO_2 surface displays a rich surface chemistry of the interfacial Lewis acidic, Lewis basic species, and Bronsted acidic sites and afterwards induces a strong adsorption of various small molecules and ions (CO_2, H_2O, ions in media, etc.). They no doubting change the surface properties and affect the catalytic performance. However, the state-of-the-art investigation ignores the contributions of those adsorbed species, which might cause the misunderstandings on the catalytic mechanisms. Thus, it is pivotal to develop new methods and theory to probe the surface states of CeO_2 and to tailor the surface physicochemical properties of CeO_2. Especially, theoretical calculations can provide the primary cognitions of those adsorbates and in turn guide the experiments to give a deep sight on catalytic mechanism.

(5) The development of theoretical methodologies can guide the rational design of highly performed CeO_2 nanozymes. Theoretical calculations are generally adopted to simulate the catalytic behavior of heterogeneous catalysts and guide catalyst

design by minimizing experiments. However, majority of the current theoretical investigations on CeO_2 nanozymes always simplify the model of CeO_2 surface, and neglect the oxygen mobility in lattice without considering the complicatedly realistic operations conditions, leading to the raised disagreements between experimental observations and calculations or between two different theoretical studies. Therefore, advanced theoretical methodologies are expected to mimic the realistic surface of CeO_2 catalysts and catalytic environments to offer the insightful understandings on the enzyme-like catalytic mechanism of CeO_2.

Acknowledgements

This work was financially supported by the National Natural Science Foundation of China (Nos. 21872109 and 52002314) and China Postdoctoral Science Foundation (Nos. 2018M633504 and 2018M633749). Authors also acknowledge the support from the Fundamental Research Funds for the Central Universities (Nos. D5000210829, D5000210601, and G2021KY05102) and Funds Shaanxi Province (No. 2021JM-589).

References

[1] Liang, M. M.; Yan, X. Y. Nanozymes: From new concepts, mechanisms, and standards to applications. *Acc. Chem. Res.* **2019**, *52*, 2190–2200.

[2] Wu, J. J. X.; Wang, X. Y.; Wang, Q.; Lou, Z. P.; Li, S. R.; Zhu, Y. Y.; Qin, L.; Wei, H. Nanomaterials with enzyme-like characteristics (nanozymes): Next-generation artificial enzymes(II). *Chem. Soc. Rev.* **2019**, *48*, 1004–1076.

[3] Huang, Y. Y.; Ren, J. S.; Qu, X. G. Nanozymes: Classification, catalytic mechanisms, activity regulation, and applications. *Chem. Rev.* **2019**, *119*, 4357–4412.

[4] Fedeli, S.; Im, J.; Gopalakrishnan, S.; Elia, J. L.; Gupta, A.; Kim, D.; Rotello, V. M. Nanomaterial-based bioorthogonal nanozymes for biological applications. *Chem. Soc. Rev.* **2021**, *50*, 13467–13480.

[5] Jiang, D. W.; Ni, D. L.; Rosenkrans, Z. T.; Huang, P.; Yan, X. Y.; Cai, W. B. Nanozyme: New horizons for responsive biomedical applications. *Chem. Soc. Rev.* **2019**, *48*, 3683–3704.

[6] Mujtaba, J.; Liu, J. R.; Dey, K. K.; Li, T. L.; Chakraborty, R.; Xu, K. L.; Makarov, D.; Barmin, R. A.; Gorin, D. A.; Tolstoy, V. P. et al. Micro-bio-chemo-mechanical-systems: Micromotors, microfluidics, and nanozymes for biomedical applications. *Adv. Mater.* **2021**, *33*, 2007465.

[7] Gao, L. Z.; Zhuang, J.; Nie, L.; Zhang, J. B.; Zhang, Y.; Gu, N.; Wang, T. H.; Feng, J.; Yang, D. L.; Perrett, S. et al. Intrinsic peroxidase-like activity of ferromagnetic nanoparticles. *Nat. Nanotechnol.* **2007**, *2*, 577–583.

[8] Ai, Y. J.; Hu, Z. N.; Liang, X. P.; Sun, H. B.; Xin, H. B.; Liang, Q. L. Recent advances in nanozymes: From matters to bioapplications. *Adv. Fun. Mater.* **2022**, *32*, 2110432.

[9] Han, J. J.; Gong, H. N.; Ren, X. K.; Yan, X. H. Supramolecular nanozymes based on peptide self-assembly for biomimetic catalysis. *Nano Today* **2021**, *41*, 101295.

[10] Zhang, X. L.; Li, G. L.; Chen, G.; Wu, D.; Wu, Y. N.; James, T. D. Enzyme mimics for engineered biomimetic cascade nanoreactors: Mechanism, applications, and prospects. *Adv. Fun. Mater.* **2021**, *31*, 2106139.

[11] Liu, S. D.; Xu, J. Y.; Xing, Y. P.; Yan, T. F.; Yu, S. J.; Sun, H. C.; Liu, J. Q. Nanozymes as efficient tools for catalytic therapeutics. *View* **2022**, *3*, 20200147.

[12] Zhang, R. F.; Yan, X. Y.; Fan, K. L. Nanozymes inspired by natural enzymes. *Acc. Mater. Res.* **2021**, *2*, 534–547.

[13] Li, Y. Q.; Liu, J. W. Nanozyme's catching up: Activity, specificity, reaction conditions and reaction types. *Mater. Horiz.* **2021**, *8*, 336–350.

[14] Zu, Y.; Yao, H. Q.; Wang, Y. F.; Yan, L.; Gu, Z. J.; Chen, C. Y.; Gao, L. Z.; Yin, W. Y. The age of bioinspired molybdenum-involved nanozymes: Synthesis, catalytic mechanisms, and biomedical applications. *View* **2021**, *2*, 20200188.

[15] Ding, H.; Hu, B.; Zhang, B.; Zhang, H.; Yan, X. Y.; Nie, G. H.; Liang, M. M. Carbon-based nanozymes for biomedical applications. *Nano Res.* **2021**, *14*, 570–583.

[16] Shen, L. H.; Ye, D. X.; Zhao, H. B.; Zhang, J. J. Perspectives for single-atom nanozymes: Advanced synthesis, functional mechanisms, and biomedical applications. *Anal. Chem.* **2021**, *93*, 1221–1231.

[17] Zhou, Y.; Wei, Y.; Ren, J. S.; Qu, X. G. A chiral covalent organic framework (COF) nanozyme with ultrahigh enzymatic activity. *Mater. Horiz.* **2020**, *7*, 3291–3297.

[18] Ma, L.; Jiang, F. B.; Fan, X.; Wang, L. Y.; He, C.; Zhou, M.; Li, S.; Luo, H. R.; Cheng, C.; Qiu, L. Metal-organic-framework-engineered enzyme-mimetic catalysts. *Adv. Mater.* **2020**, *32*, 2003065.

[19] Wang, D. D.; Jana, D.; Zhao, Y. L. Metal-organic framework derived nanozymes in biomedicine. *Acc. Chem. Res.* **2020**, *53*, 1389–1400.

[20] Mikolajczak, D. J.; Berger, A. A.; Koksch, B. Catalytically active peptide-gold nanoparticle conjugates: Prospecting for artificial enzymes. *Angew. Chem., Int. Ed.* **2020**, *59*, 8776–8785.

[21] Meng, Y. T.; Li, W. F.; Pan, X. L.; Gadd, G. M. Applications of nanozymes in the environment. *Environ. Sci. Nano* **2020**, *7*, 1305–1318.

[22] Liu, X. L.; Gao, Y.; Chandrawati, R.; Hosta-Rigau, L. Therapeutic applications of multifunctional nanozymes. *Nanoscale* **2019**, *11*, 21046–21060.

[23] Wang, Q. Q.; Wei, H.; Zhang, Z. Q.; Wang, E. K.; Dong, S. J. Nanozyme: An emerging alternative to natural enzyme for biosensing and immunoassay. *TrAC Trends Anal. Chem.* **2018**, *105*, 218–224.

[24] Cormode, D. P.; Gao, L. Z.; Koo, H. Emerging biomedical applications of enzyme-like catalytic nanomaterials. *Trends Biotechnol.* **2018**, *36*, 15–29.

[25] Wang, H.; Wan, K. W.; Shi X. H. Recent advances in nanozyme research. *Adv. Mater.* **2019**, *31*, 1805368.

[26] Jiang, B.; Duan, D. M.; Gao, L. Z.; Zhou, M. J.; Fan, K. L.; Tang, Y.; Xi, J. Q.; Bi, Y. H.; Tong, Z.; Gao, G. F. et al. Standardized assays for determining the catalytic activity and kinetics of peroxidase-like nanozymes. *Nat. Protoc.* **2018**, *13*, 1506–1520.

[27] Liu, Q.; Wan, K. W.; Shang, Y. X.; Wang, Z. G.; Zhang, Y. Y.; Dai, L. R.; Wang, C.; Wang, H.; Shi, X. H.; Liu, D. S. et al. Cofactor-free oxidase-mimetic nanomaterials from self-assembled histidine-rich peptides. *Nat. Mater.* **2021**, *20*, 395–402.

[28] Lu, W. H.; Yuan, M.; Chen, J.; Zhang, J. X.; Kong, L. S.; Feng, Z. Y.; Ma, X. C.; Su, J.; Zhan, J. H. Synergistic Lewis acid-base sites of ultrathin porous Co_3O_4 nanosheets with enhanced peroxidase-like activity. *Nano Res.* **2021**, *14*, 3514–3522.

[29] Zhou, Q.; Yang, H.; Chen, X. H.; Xu, Y.; Han, D.; Zhou, S. S.; Liu, S. Q.; Shen, Y. F.; Zhang, Y. J. Cascaded nanozyme system with high reaction selectivity by substrate screening and channeling in a microfluidic device. *Angew. Chem., Int. Ed.* **2022**, *134*, e202112453.

[30] Cao, S. J.; Zhao, Z. Y.; Zheng, Y. J.; Wu, Z. H.; Ma, T.; Zhu, B. H.; Yang, C. D.; Xiang, X.; Ma, L.; Han, X. L. et al. A library of ROS-catalytic metalloenzyme mimics with atomic metal centers. *Adv. Mater.* **2022**, *34*, 2200255.

[31] Liu, B. W.; Liu, J. W. Surface modification of nanozymes. *Nano Res.* **2017**, *10*, 1125–1148.

[32] Perez, J. M.; Asati, A.; Nath, S.; Kaittanis, C. Synthesis of biocompatible dextran-coated nanoceria with pH-dependent antioxidant properties. *Small* **2008**, *4*, 552–556.

[33] Karakoti, A. S.; Singh, S.; Kumar, A.; Malinska, M.; Kuchibhatla, S. V. N. T.; Wozniak, K.; Self, W. T.; Seal, S. PEGylated nanoceria as radical scavenger with tunable redox chemistry. *J. Am. Chem. Soc.* **2009**, *131*, 14144–14145.

[34] Asati, A.; Santra, S.; Kaittanis, C.; Nath, S.; Perez, J. M. Oxidase-like activity of polymer-coated cerium oxide nanoparticles. *Angew. Chem.* **2009**, *121*, 2344–2348.

[35] Singh, S.; Dosani, T.; Karakoti, A. S.; Kumar, A.; Seal, S.; Self, W.

T. A phosphate-dependent shift in redox state of cerium oxide nanoparticles and its effects on catalytic properties. *Biomaterials* **2011**, *32*, 6745–6753.

[36] Tan, Z. C.; Li, G. C.; Chou, H. L.; Li, Y. Y.; Yi, X. F.; Mahadi, A. H.; Zheng, A. M.; Tsang, S. C. E.; Peng, Y. K. Differentiating surface Ce species among CeO_2 facets by solid-state NMR for catalytic correlation. *ACS Catal.* **2020**, *10*, 4003–4011.

[37] Niu, X. H.; Xu, X. C.; Li, X.; Pan, J. M.; Qiu, F. X.; Zhao, H. L.; Lan, M. B. Surface charge engineering of nanosized CuS via acidic amino acid modification enables high peroxidase-mimicking activity at neutral pH for one-pot detection of glucose. *Chem. Commun.* **2018**, *54*, 13443–13446.

[38] Xue, Y.; Zhai, Y. W.; Zhou, K. B.; Wang, L.; Tan, H. N.; Luan, Q. F.; Yao, X. The vital role of buffer anions in the antioxidant activity of CeO_2 nanoparticles. *Chem.—Eur. J.* **2012**, *18*, 11115–11122.

[39] Baldim, V.; Bedioui, F.; Mignet, N.; Margaill, I.; Berret, J. F. The enzyme-like catalytic activity of cerium oxide nanoparticles and its dependency on Ce^{3+} surface area concentration. *Nanoscale* **2018**, *10*, 6971–6980.

[40] Li, Y. Y.; He, X.; Yin, J. J.; Ma, Y. H.; Zhang, P.; Li, J. Y.; Ding, Y. Y.; Zhang, J.; Zhao, Y. L.; Chai, Z. F. et al. Acquired superoxide-scavenging ability of ceria nanoparticles. *Angew. Chem., Int. Ed.* **2015**, *54*, 1832–1835.

[41] Tian, Z. M.; Li, J.; Zhang, Z. Y.; Gao, W. M.; Zhou, X. Q.; Qu, Y. Q. Highly sensitive and robust peroxidase-like activity of porous nanorods of ceria and their application for breast cancer detection. *Biomaterials* **2015**, *59*, 116–124.

[42] Tian, Z. M.; Li, X. H.; Ma, Y. Y.; Chen, T.; Xu, D. H.; Wang, B. C.; Qu, Y. Q.; Gao, Y. Quantitatively intrinsic biomimetic catalytic activity of nanocerias as radical scavengers and their ability against H_2O_2 and doxorubicin-induced oxidative stress. *ACS Appl. Mater. Interfaces* **2017**, *9*, 23342–23352.

[43] Tian, Z. M.; Liu, H. B.; Guo, Z. X.; Gou, W. Y.; Liang, Z. C.; Qu, Y. Q.; Han, L. L.; Liu, L. A pH-responsive polymer-CeO_2 hybrid to catalytically generate oxidative stress for tumor therapy. *Small* **2020**, *16*, 2004654.

[44] Cao, F. X.; Zhang, M. K.; Yang, K. L.; Tian, Z. M.; Li, J.; Qu, Y. Q. Single crystalline CeO_2 nanotubes. *Nano Res.* **2021**, *14*, 715–719.

[45] Lee, S. S.; Song, W. S.; Cho, M.; Puppala, H. L.; Nguyen, P.; Zhu, H. G.; Segatori, L.; Colvin, V. L. Antioxidant properties of cerium oxide nanocrystals as a function of nanocrystal diameter and surface coating. *ACS Nano* **2013**, *7*, 9693–9703.

[46] Liu, Y.; Purich, D. L.; Wu, C. C.; Wu, Y.; Chen, T.; Cui, C.; Zhang, L. Q.; Cansiz, S.; Hou, W. J.; Wang, Y. Y. et al. Ionic functionalization of hydrophobic colloidal nanoparticles to form ionic nanoparticles with enzymelike properties. *J. Am. Chem. Soc.* **2015**, *137*, 14952–14958.

[47] Fan, K. L.; Wang, H.; Xi, J. Q.; Liu, Q.; Meng, X. Q.; Duan, D. M.; Gao, L. Z.; Yan, X. Y. Optimization of Fe_3O_4 nanozyme activity via single amino acid modification mimicking an enzyme active site. *Chem. Commun.* **2017**, *53*, 424–427.

[48] Zhang, L.; Liu, Z. W.; Deng, Q. Q.; Sang, Y. J.; Dong, K.; Ren, J. S.; Qu, X. G. Nature-inspired construction of MOF@COF nanozyme with active sites in tailored microenvironment and pseudopodia-like surface for enhanced bacterial inhibition. *Angew. Chem., Int. Ed.* **2021**, *60*, 3469–3474.

[49] Cao-Milán, R.; He, L. D.; Shorkey, S.; Tonga, G. Y.; Wang, L. S.; Zhang, X. Z.; Uddin, I.; Das, R.; Sulak, M.; Rotello, V. M. Modulating the catalytic activity of enzyme-like nanoparticles through their surface functionalization. *Mol. Syst. Des. Eng.* **2017**, *2*, 624–628.

[50] Bülbül, G.; Hayat, A.; Andreescu, S. ssDNA-functionalized nanoceria: A redox-active aptaswitch for biomolecular recognition. *Adv. Healthc. Mater.* **2016**, *5*, 822–828.

[51] Lin, Y. H.; Huang, Y. Y.; Ren, J. S.; Qu, X. G. Incorporating ATP into biomimetic catalysts for realizing exceptional enzymatic performance over a broad temperature range. *NPG Asia Mater.* **2014**, *6*, e114.

[52] Park, K. S.; Kim, M. I.; Cho, D. Y.; Park, H. G. Label-free colorimetric detection of nucleic acids based on target-induced shielding against the peroxidase-mimicking activity of magnetic nanoparticles. *Small* **2011**, *7*, 1521–1525.

[53] Sun, H. J.; Zhao, A. D.; Gao, N.; Li, K.; Ren, J. S.; Qu, X. G. Deciphering a nanocarbon-based artificial peroxidase: Chemical identification of the catalytically active and substrate-binding sites on graphene quantum dots. *Angew. Chem., Int. Ed.* **2015**, *54*, 7176–7180.

[54] Lord, M. S.; Berret, J. F.; Singh, S.; Vinu, A.; Karakoti, A. S. Redox active cerium oxide nanoparticles: Current status and burning issues. *Small* **2021**, *17*, 2102342.

[55] Xu, C.; Qu, X. G. Cerium oxide nanoparticle: A remarkably versatile rare earth nanomaterial for biological applications. *NPG Asia Mater.* **2014**, *6*, e90.

[56] Saifi, M. A.; Seal, S.; Godugu, C. Nanoceria, the versatile nanoparticles: Promising biomedical applications. *J. Control. Release* **2021**, *338*, 164–189.

[57] Das, S.; Dowding, J. M.; Klump, K. E.; McGinnis, J. F.; Self, W.; Seal, S. Cerium oxide nanoparticles: Applications and prospects in nanomedicine. *Nanomedicine* **2013**, *8*, 1483–1508.

[58] Das, M.; Patil, S.; Bhargava, N.; Kang, J. F.; Riedel, L. M.; Seal, S.; Hickman, J. J. Auto-catalytic ceria nanoparticles offer neuroprotection to adult rat spinal cord neurons. *Biomaterials* **2007**, *28*, 1918–1925.

[59] Tian, Z. M.; Zhao, J. L.; Zhao, S. J.; Li, H. C.; Guo, Z. X.; Liang, Z. C.; Li, J. Y.; Qu, Y. Q. Phytic acid-modified CeO_2 as Ca^{2+} inhibitor for a security reversal of tumor drug resistance. *Nano Res.* **2022**, *15*, 4334–4343.

[60] Yao, T. Z.; Tian, Z. M.; Zhang, Y. Q.; Qu, Y. Q. Phosphatase-like activity of porous nanorods of CeO_2 for the highly stabilized dephosphorylation under interferences. *ACS Appl. Mater. Interfaces* **2019**, *11*, 195–201.

[61] Tian, Z. M.; Yao, T. Z.; Qu, C. Y.; Zhang, S.; Li, X. H.; Qu, Y. Q. Photolyase-like catalytic behavior of CeO_2. *Nano Lett.* **2019**, *19*, 8270–8277.

[62] Herget, K.; Hubach, P.; Pusch, S.; Deglmann, P.; Götz, H.; Gorelik, T. E.; Gural'skiy, I. A.; Pfitzner, F.; Link, T.; Schenk, S. et al. Haloperoxidase mimicry by CeO_{2-x} nanorods combats biofouling. *Adv. Mater.* **2017**, *29*, 1603823.

[63] Zambon, A.; Malavasi, G.; Pallini, A.; Fraulini, F.; Lusvardi, G. Cerium containing bioactive glasses: A review. *ACS Biomater. Sci. Eng.* **2021**, *7*, 4388–4401.

[64] Dong, H. J.; Fan, Y. Y.; Zhang, W.; Gu, N.; Zhang, Y. Catalytic mechanisms of nanozymes and their applications in biomedicine. *Bioconjugate Chem.* **2019**, *30*, 1273–1296.

[65] Zandieh, M.; Liu, J. W. Surface science of nanozymes and defining a nanozyme unit. *Langmuir* **2022**, *38*, 3617–3622.

[66] Seal, S.; Jeyaranjan, A.; Neal, C. J.; Kumar, U.; Sakthivel, T. S.; Sayle, D. C. Engineered defects in cerium oxides: Tuning chemical reactivity for biomedical, environmental, & energy applications. *Nanoscale* **2020**, *12*, 6879–6899.

[67] Celardo, I.; Pedersen, J. Z.; Traversa, E.; Ghibelli, L. Pharmacological potential of cerium oxide nanoparticles. *Nanoscale* **2011**, *3*, 1411–1420.

[68] Zahra, D.; Javaid, A.; Iqbal, M.; Akbar, I.; Ashfaq, U. A. Synthesis and therapeutic potential of nanoceria against cancer: An update. *Crit. Rev. Ther. Drug Carrier Syst.* **2021**, *38*, 1–26.

[69] Hosseini, M.; Mozafari, M. Cerium oxide nanoparticles: Recent advances in tissue engineering. *Materials* **2020**, *13*, 3072.

[70] Ma, Y. Y.; Gao, W.; Zhang, Z. Y.; Zhang, S.; Tian, Z. M.; Liu, Y. X.; Ho, J. C.; Qu, Y. Q. Regulating the surface of nanoceria and its applications in heterogeneous catalysis. *Surf. Sci. Rep.* **2018**, *73*, 1–36.

[71] Zhang, S.; Xia, Z. M.; Zou, Y.; Cao, F. X.; Liu, Y. X.; Ma, Y. Y.; Qu, Y. Q. Interfacial frustrated Lewis pairs of CeO_2 activate CO_2 for selective tandem transformation of olefins and CO_2 into cyclic carbonates. *J. Am. Chem. Soc.* **2019**, *141*, 11353–11357.

[72] Zhang, S.; Huang, Z. Q.; Ma, Y. Y.; Gao, W.; Li, J.; Cao, F. X.; Li, L.; Chang, C. R.; Qu, Y. Q. Solid frustrated-Lewis-pair catalysts constructed by regulations on surface defects of porous nanorods of

CeO_2. *Nat. Commun.* **2017**, *8*, 15266.
[73] Gao, W.; Xia, Z. M.; Cao, F. X.; Ho, J. C.; Jiang, Z.; Qu, Y. Q. Comprehensive understanding of the spatial configurations of CeO_2 in NiO for the electrocatalytic oxygen evolution reaction: Embedded or surface-loaded. *Adv. Fun. Mater.* **2018**, *28*, 1706056.
[74] Schmitt, R.; Nenning, A.; Kraynis, O.; Korobko, R.; Frenkel, A. I.; Lubomirsky, I.; Haile, S. M.; Rupp, J. L. M. A review of defect structure and chemistry in ceria and its solid solutions. *Chem. Soc. Rev.* **2020**, *49*, 554–592.
[75] Wu, K.; Sun, L. D.; Yan, C. H. Recent progress in well-controlled synthesis of ceria-based nanocatalysts towards enhanced catalytic performance. *Adv. Energy Mater.* **2016**, *6*, 1600501.
[76] Campbell, C. T.; Peden, C. H. F. Oxygen vacancies and catalysis on ceria surfaces. *Science* **2005**, *309*, 713–714.
[77] Zhang, Y.; Zhao, S. N.; Feng, J.; Song, S. Y.; Shi, W. D.; Wang, D.; Zhang, H. J. Unraveling the physical chemistry and materials science of CeO_2-based nanostructures. *Chem* **2021**, *7*, 2022–2059.
[78] Ziemba, M.; Schilling, C.; Ganduglia-Pirovano, M. V.; Hess, C. Toward an atomic-level understanding of ceria-based catalysts: When experiment and theory go hand in hand. *Acc. Chem. Res.* **2021**, *54*, 2884–2893.
[79] Xu, Y. W.; Mofarah, S. S.; Mehmood, R.; Cazorla, C.; Koshy, P.; Sorrell, C. C. Design strategies for ceria nanomaterials: Untangling key mechanistic concepts. *Mater. Horiz.* **2021**, *8*, 102–123.
[80] Ma, J. L.; Ye, F.; Ou, D. R.; Li, L. L.; Mori, T. Structures of defect clusters on ceria {111} surface. *J. Phys. Chem. C* **2012**, *116*, 25777–25782.
[81] Liu, X. W.; Zhou, K. B.; Wang, L.; Wang, B. Y.; Li, Y. D. Oxygen vacancy clusters promoting reducibility and activity of ceria nanorods. *J. Am. Chem. Soc.* **2009**, *131*, 3140–3141.
[82] Schilling, C.; Ganduglia-Pirovano, M. V.; Hess, C. Experimental and theoretical study on the nature of adsorbed oxygen species on shaped ceria nanoparticles. *J. Phys. Chem. Lett.* **2018**, *9*, 6593–6598.
[83] Trovarelli, A.; Llorca, J. Ceria catalysts at nanoscale: How do crystal shapes shape catalysis? *ACS Catal.* **2017**, *7*, 4716–4735.
[84] Vayssilov, G. N.; Migani, A.; Neyman, K. Density functional modeling of the interactions of platinum clusters with CeO_2 nanoparticles of different size. *J. Phys. Chem. C* **2011**, *115*, 16081–16086.
[85] Berestok, T.; Guardia, P.; Blanco, J.; Nafria, R.; Torruella, P.; López-Conesa, L.; Estradé, S.; Ibáñez, M.; De Roo, J.; Luo, Z. S. et al. Tuning branching in ceria nanocrystals. *Chem. Mater.* **2017**, *29*, 4418–4424.
[86] Nolan, M. Enhanced oxygen vacancy formation in ceria (111) and (110) surfaces doped with divalent cations. *J. Mater. Chem.* **2011**, *21*, 9160–9168.
[87] Nolan, M.; Parker, S. C.; Watson, G. W. The electronic structure of oxygen vacancy defects at the low index surfaces of ceria. *Surf. Sci.* **2005**, *595*, 223–232.
[88] Wu, Z. L.; Li, M. J.; Overbury, S. H. On the structure dependence of CO oxidation over CeO_2 nanocrystals with well-defined surface planes. *J. Catal.* **2012**, *285*, 61–73.
[89] Cargnello, M.; Doan-Nguyen, V. V. T.; Gordon, T. R.; Diaz, R. E.; Stach, E. A.; Gorte, R. J.; Fornasiero, P.; Murray, C. B. Control of metal nanocrystal size reveals metal-support interface role for ceria catalysts. *Science* **2013**, *341*, 771–773.
[90] Mai, H. X.; Sun, L. D.; Zhang, Y. W.; Si, R.; Feng, W.; Zhang, H. P.; Liu, H. C.; Yan, C. H. Shape-selective synthesis and oxygen storage behavior of ceria nanopolyhedra, nanorods, and nanocubes. *J. Phys. Chem. B* **2005**, *109*, 24380–24385.
[91] Lin, F.; Hoang, D. T.; Tsung, C. K.; Huang, W. Y.; Lo. S. H. Y.; Wood, J. B.; Wang, H.; Tang, J. Y.; Yang, P. D. Catalytic properties of Pt cluster-decorated CeO_2 nanostructures. *Nano Res.* **2011**, *4*, 61–71.
[92] Ji, Z. X.; Wang, X.; Zhang, H. Y.; Lin, S. J.; Meng, H.; Sun, B. B.; George, S.; Xia, T.; Nel, A. E.; Zink, J. I. Designed synthesis of CeO_2 nanorods and nanowires for studying toxicological effects of high aspect ratio nanomaterials. *ACS Nano* **2012**, *6*, 5366–5380.
[93] Gao, W.; Li, J.; Zhou, X. M.; Zhang, Z. Y.; Ma, Y. Y.; Qu, Y. Q. Repeatable fluorescence switcher of Eu^{3+}-doped CeO_2 nanorods by L(+)-ascorbic acid and hydrogen peroxide. *J. Mater. Chem. C* **2014**, *2*, 8729–8735.
[94] Li, J.; Zhang, Z. Y.; Gao, W.; Zhang, S.; Ma, Y. Y.; Qu Y. Q. Pressure regulations on the surface properties of CeO_2 nanorods and their catalytic activity for CO oxidation and nitrile hydrolysis reactions. *ACS Appl. Mater. Interfaces* **2016**, *8*, 22988–22996.
[95] Tan, Z. C.; Wu, T. S.; Soo, Y. L.; Peng, Y. K. Unravelling the true active site for CeO_2-catalyzed dephosphorylation. *Appl. Catal. B Environ.* **2020**, *264*, 118508.
[96] Zhang, J. R.; Tan, Z. C.; Leng, W. Y.; Chen, Y. C.; Zhang, S. Q.; Lo, B. T. W.; Yung, K. K. L.; Peng, Y. K. Chemical state tuning of surface Ce species on pristine CeO_2 with 2400% boosting in peroxidase-like activity for glucose detection. *Chem. Commun.* **2020**, *56*, 7897–7900.
[97] Wang, Z. Z.; Shen, X. M.; Gao, X. F. Density functional theory mechanistic insight into the peroxidase- and oxidase-like activities of nanoceria. *J. Phys. Chem. C* **2021**, *125*, 23098–23104.
[98] Nguyen, P. T.; Lee, J.; Cho, A.; Kim, M. S.; Choi, D.; Han, J. W.; Kim, M. I.; Lee, J. Rational development of Co-doped mesoporous ceria with high peroxidase-mimicking activity at neutral pH for paper-based colorimetric detection of multiple biomarkers. *Adv. Funct. Mater.* **2022**, *32*, 2112428.
[99] Dong, S. M.; Dong, Y. S.; Liu, B.; Liu, J.; Liu, S. K.; Zhao, Z. Y.; Li, W. T.; Tian, B. S.; Zhao, R. X.; He, F. et al. Guiding transition metal-doped hollow cerium tandem nanozymes with elaborately regulated multi-enzymatic activities for intensive chemodynamic therapy. *Adv. Mater.* **2022**, *34*, 2107054.
[100] Cheng, F.; Wang, S. Q.; Zheng, H.; Yang, S. W.; Zhou, L.; Liu, K. K.; Zhang, Q. Y.; Zhang, H. P. Cu-doped cerium oxide-based nanomedicine for tumor microenvironment-stimulative chemo-chemodynamic therapy with minimal side effects. *Colloids Surf. B Biointerfaces* **2021**, *205*, 111878.
[101] Tan, Z. C.; Zhang, J. R.; Chen, Y. C.; Chou, J. P.; Peng, Y. K. Unravelling the role of structural geometry and chemical state of well-defined oxygen vacancies on pristine CeO_2 for H_2O_2 activation. *J. Phys. Chem. Lett.* **2020**, *11*, 5390–5396.
[102] Wang, Y. H.; Wang, F.; Song, Q.; Xin, Q.; Xu, S. T.; Xu, J. Heterogeneous ceria catalyst with water-tolerant Lewis acidic sites for one-pot synthesis of 1, 3-diols via Prins condensation and hydrolysis reactions. *J. Am. Chem. Soc.* **2013**, *135*, 1506–1515.
[103] Baldim, V.; Yadav, N.; Bia, N.; Graillot, A.; Loubat, C.; Singh, S.; Karakoti, A. S.; Berret, J. F. Polymer-coated cerium oxide nanoparticles as oxidoreductase-like catalysts. *ACS Appl. Mater. Interfaces* **2020**, *12*, 42056–42066.
[104] Zhao, Y. L.; Wang, Y. W.; Mathur, A.; Wang, Y. Q.; Maheshwari, V.; Su, H. J.; Liu, J. W. Fluoride-capped nanoceria as a highly efficient oxidase-mimicking nanozyme: Inhibiting product adsorption and increasing oxygen vacancies. *Nanoscale* **2019**, *11*, 17841–17850.
[105] Celardo, I.; De Nicola, M.; Mandoli, C.; Pedersen, J. Z.; Traversa, E.; Ghibelli, L. Ce^{3+} ions determine redox-dependent anti-apoptotic effect of cerium oxide nanoparticles. *ACS Nano* **2011**, *5*, 4537–4549.
[106] Heckert, E. G.; Karakoti, A. S.; Seal, S.; Self, W. T. The role of cerium redox state in the SOD mimetic activity of nanoceria. *Biomaterials* **2008**, *29*, 2705–2709.
[107] Korsvik, C.; Patil, S.; Seal, S.; Self, W. T. Superoxide dismutase mimetic properties exhibited by vacancy engineered ceria nanoparticles. *Chem. Commun.* **2007**, 1056–1058.
[108] Wang, Z. Z.; Shen, X. M.; Gao, X. F.; Zhao, Y. L. Simultaneous enzyme mimicking and chemical reduction mechanisms for nanoceria as a bio-antioxidant: A catalytic model bridging computations and experiments for nanozymes. *Nanoscale* **2019**, *11*, 13289–13299.
[109] Pirmohamed, T.; Dowding, J. M.; Singh, S.; Wasserman, B.; Heckert, E.; Karakoti, A. S.; King, J. E. S.; Seal, S.; Self, W. T. Nanoceria exhibit redox state-dependent catalase mimetic activity. *Chem. Commun.* **2010**, *46*, 2736–2738.
[110] Yao, C.; Wang, W. X.; Wang, P. Y.; Zhao, M. Y.; Li, X. M.; Zhang, F. Near-infrared upconversion mesoporous cerium oxide hollow biophotocatalyst for concurrent pH-/H_2O_2-responsive O_2-

evolving synergetic cancer therapy. *Adv. Mater.* **2018**, *30*, 1704833.
[111] Weng, Q. J.; Sun, H.; Fang, C. Y.; Xia, F.; Liao, H. W.; Lee, J.; Wang, J. C.; Xie, A.; Ren, J. F.; Guo, X. et al. Catalytic activity tunable ceria nanoparticles prevent chemotherapy-induced acute kidney injury without interference with chemotherapeutics. *Nat. Commun.* **2021**, *12*, 1436.
[112] Ni, D. L.; Wei, H.; Chen, W. Y.; Bao, Q. Q.; Rosenkrans, Z. T.; Barnhart T. E.; Ferreira, C. A.; Wang, Y. P.; Yao, H. L.; Sun, T. W. et al. Ceria Nanoparticles meet hepatic ischemia-reperfusion injury: The perfect imperfection. *Adv. Mater.* **2019**, *31*, 1902956.
[113] Soh, M.; Kang, D. W.; Jeong, H. G.; Kim, D.; Kim, D. Y.; Yang, W.; Song, C.; Baik, S.; Choi, I. Y.; Ki, S. K. et al. Ceria-zirconia nanoparticles as an enhanced multi-antioxidant for sepsis treatment. *Angew. Chem., Int. Ed.* **2017**, *56*, 11399–11403.
[114] Sancar, A. Structure and function of DNA photolyase and cryptochrome blue-light photoreceptors. *Chem. Rev.* **2003**, *103*, 2203–2238.
[115] Thiagarajan, V.; Byrdin, M.; Eker, A. P. M.; Müller, P.; Brettel, K. Kinetics of cyclobutane thymine dimer splitting by DNA photolyase directly monitored in the UV. *Proc. Natl. Acad. Sci. USA* **2011**, *108*, 9402–9407.
[116] Bucher, D. B.; Kufner, C. L.; Schlueter, A.; Carell, T.; Zinth, W. UV-induced charge transfer states in DNA promote sequence selective self-repair. J. Am. *Chem. Soc.* **2016**, *138*, 186–190.
[117] Rousseau, B. J. G.; Shafei, S.; Migliore, A.; Stanley, R. J.; Beratan, D. N. Determinants of photolyase's DNA repair mechanism in mesophiles and extremophiles. *J. Am. Chem. Soc.* **2018**, *140*, 2853–2861.
[118] Manto, M. J.; Xie, P. F.; Wang, C. Catalytic dephosphorylation using ceria nanocrystals. *ACS Catal.* **2017**, *7*, 1931–1938.
[119] Liu, H. Y.; Liu, J. W. Self-limited phosphatase-mimicking CeO_2 nanozymes. *ChemNanoMat* **2020**, *6*, 947–952.
[120] Kuchma, M. H.; Komanski, C. B.; Colon, J.; Teblum, A.; Masunov, A. E.; Alvarado, B.; Babu, S.; Seal, S.; Summy, J.; Baker, C. H. Phosphate ester hydrolysis of biologically relevant molecules by cerium oxide nanoparticles. *Nanomedicine* **2010**, *6*, 738–744.
[121] Zhao, C. L.; Xu, Y. Theoretical investigation of dephosphorylation of phosphate monoesters on CeO_2 (111). *Catal. Today* **2018**, *312*, 141–148.
[122] Janoš, P.; Ederer, J.; Došek, M.; Štojdl, J.; Henych, J.; Tolasz, J.; Kormunda, M.; Mazanec, K. Can cerium oxide serve as a phosphodiesterase-mimetic nanozyme? *Environ. Sci. Nano* **2019**, *6*, 3684–3698.
[123] Butler, A.; Sandy, M. Mechanistic considerations of halogenating enzymes. *Nature* **2009**, *460*, 848–854.
[124] Frerichs, H.; Pütz, E.; Pfitzner, F.; Reich, T.; Gazanis, A.; Panthöfer, M.; Hartmann, J.; Jegel, O.; Heermann, R.; Tremel, W. Nanocomposite antimicrobials prevent bacterial growth through the enzyme-like activity of Bi-doped cerium dioxide ($Ce_{1-x}Bi_xO_{2-\delta}$). *Nanoscale* **2020**, *12*, 21344–21358.
[125] Hu, M. H.; Korschelt, K.; Viel, M.; Wiesmann, N.; Kappl, M.; Brieger, J.; Landfester, K.; Thérien-Aubin, H.; Tremel, W. Nanozymes in nanofibrous mats with haloperoxidase-like activity to combat biofouling. *ACS Appl. Mater. Interfaces* **2018**, *10*, 44722–44730.
[126] Lang, J. Y.; Ma, X. J.; Chen, P. Y.; Serota, M. D.; Andre, N. M.; Whittaker, G. R.; Yang, R. Haloperoxidase-mimicking CeO_{2-x} nanorods for the deactivation of human coronavirus OC43. *Nanoscale* **2022**, *14*, 3731–3737.
[127] Xu, F.; Lu, Q. W.; Huang, P. J. J.; Liu, J. W. Nanoceria as a DNase I mimicking nanozyme. *Chem. Commun.* **2019**, *55*, 13215–13218.
[128] Korschelt, K.; Schwidetzky, R.; Pfitzner, F.; Strugatchi, J.; Schilling, C.; von der Au, M.; Kirchhoff, K.; Panthöfer, M.; Lieberwirth, I.; Tahir, M. N. et al. CeO_{2-x} nanorods with intrinsic urease-like activity. *Nanoscale* **2018**, *10*, 13074–13082.